Feedforward circuits enable modality-specific control of cortical inhibition during behavioral state transitions.

Marcel de Brito Van Velze[1], Dhanasak Dhanasobhon[1], Marie Martinez[1], Annunziato Morabito[1], Emmanuelle Berthaux[1], Cibele Martins Pinho[1], Yann Zerlaut[1#] and Nelson Rebola[1#]

[1]ICM, Paris Brain Institute, Hôpital de la Pitié-Salpêtrière, Sorbonne Université, Inserm, CNRS, Paris, 75013, France.

#These authors contributed equally.

Number of figures: 7; Supplementary figures: 4; Supplementary tables: 0

Keywords: Neocortical interneurons, Somatostatin positive Interneurons, Somatosensory cortex, Spontaneous behaviours, Locomotion, Whisking.

Acknowledgements:

This study was supported by the Centre National de la Recherche Scientifique, Agence Nationale de la Recherche (grants ANR-EXCIGLY and ANR-DecoSensoMol1) the European Research Council (ERC-STG- 678250 to N.R.), the European Union's Horizon 2020 research and innovation programme (Marie Skłodowska-Curie Grant 892175 "*InProsMod"* to Y.Z.); by the Paris Brain Institute, and the Fondation pour la Recherche Médicale (FRM; fellowship ARF201909009117 to Y.Z.). We thank the Paris Brain Institute core facilities, namely iVector and ICMice PHENOPARC. We would also like to thank Dr. Alberto Bacci (ICM, Paris), Dr. Joana Lourenco (ICM, Paris) and Dr. Nicolas Chenouard (ICM, Paris) for the valuable discussions and comments on the manuscript.

SUMMARY (236 words)

Active behavior strongly influences sensory information processing in primary sensory cortices. Local interneurons, especially those involved in disinhibitory circuits like somatostatin (SST) and vasoactive intestinal peptide (VIP)-positive interneurons, play a crucial role in regulating cortical function during behavior. While numerous studies have focused on the recruitment of pyramidal neurons, the intricate network mechanisms governing the behavior-state-dependent modulation of inhibitory neurons remain unclear. Using intravital two-photon calcium imaging we have studied the neuronal pathways that regulate SST- and VIP-IN activity in sensory cortices during spontaneous behaviours. We now reveal that active behavioral states associated with increased locomotor activity strongly recruit L2/3 SST-INs in primary somatosensory (S1) but not visual (V1) cortex indicating modality-specific mechanisms control activity of cortical interneurons during active states. Such a difference between V1 and S1 disappears in the presence of visual sensory drive (ambient light) suggesting a critical involvement of feedforward sensory pathways in the positive modulation of SST-INs during spontaneous behaviors. In agreement, we now unveil that inactivating the somatosensory thalamus significantly reduces the recruitment of SST-INs in S1 by locomotion. In contrast, interfering with disinhibitory circuits via chemogenetic inactivation of VIP-INs further increased the sensitivity of SST-INs to variations in behavioural states. Our work thus reveals a previous unknown role for thalamic inputs in driving SST-INs, suggesting that by integrating feedforward activity with neuromodulation, SST-INs play a central role in adapting sensory processing to behavioral states in a sensory modality-specific manner.

Introduction:

In the mammalian brain, the cerebral cortex is responsible for complex cognitive functions, including a coherent representation of the external world that is crucial for an effective interaction with a constantly changing environment. Importantly, sensation can occur under drastically different behavior conditions, which have been reported to result in various perceptual outcomes (Busse et al., 2017; McGinley et al., 2015a). A hallmark of sensory systems is thus to provide a flexible strategy to process incoming information in a context-dependent manner (McCormick et al., 2020).

Local neocortical interneurons, in particular those involved in disinhibitory circuits, like vasoactive intestinal peptide (VIP) and somatostatin (SST) expressing interneurons (INs), have been shown to be particularly sensitive to behavior state transitions and to be key contributors to the state-dependent regulation of cortical function (Fu et al., 2015, 2014; Gasselin et al., 2021; Gentet et al., 2012; Muñoz et al., 2017; Polack et al., 2013; Reimer et al., 2014). In V1, recruitment of VIP-INs and consequent decrease in SST-IN mediated inhibition has been suggested to underlie the gain modulation of visual-evoked responses observed during locomotion (Fu et al., 2014). Yet, the mechanisms controlling the engagement of SST-INs across active behavioral states are unclear. In addition, behavioral modulations have been shown to differentially impact pyramidal cell activity across sensory cortices (Ayaz et al., 2013; Niell and Stryker, 2010; Polack et al., 2013; Saleem et al., 2013; Schneider et al., 2014; Shimaoka et al., 2018; Vinck et al., 2015; Zhou et al., 2014). However, whether inhibitory circuits display similar or variable sensitivity to behavioral state transitions across sensory cortical areas remains unexplored.

A recent study revealed that modulation of INs activity in V1 by brain states can be largely predicted by the first transcriptomic principal component (Bugeon et al., 2022). This transcriptomic component suggested that the increase in SST-INs activity, observed in alert states, is associated with cholinergic signalling (Bugeon et al., 2022). However, this finding contrasts with a previous report that SST-INs in V1 lose cholinergic modulation during development (Yaeger et al., 2019).

108 Paradoxically, VIP-mediated disinhibition has been proposed to explain the increase in SST-INs
109 activity during active behavioral states but this hypothesis lacks experimental evidence (Garcia
110 Del Molino et al., 2017). Both hypotheses point to neuromodulatory inputs, in particular cholinergic
111 axonal projections to be at the origin of the sensitivity of VIP- and SST-INs to behavioral state
112 transitions. Yet, recent results highlighted that thalamic activity is essential for the large and
113 sustained depolarizations associated with arousal/movement-related signals in L2/3 PNs in V1
114 (Nestvogel and McCormick, 2022). These results suggest that behavior states can modulate
115 neocortical activity not only through neuromodulatory projections such as cholinergic and
116 noradrenergic pathways, but also via glutamatergic thalamic inputs. As SST-INs receive
117 pronounced inputs from local L2/3 PNs it is therefore possible that feedforward activity transmitted
118 via the thalamus participates in the behavioral-dependent modulation of SST-INs in primary
119 sensory regions. Still, as glutamatergic synapses from L2/3 PNs into SST-INs have relatively low
120 release probabilities it is unclear whether an increase in L2/3 PNs activity during active states is
121 sufficient to drive SST-INs. Altogether, the specific neuronal mechanisms governing the activity
122 of SST-INs during spontaneous behaviors are still not fully understood.

123 The modulation of disinhibitory circuits by active behavioral states has been the focus of
124 considerable scrutiny in V1 (Bugeon et al., 2022; Dipoppa et al., 2018; Fu et al., 2014; Pakan et
125 al., 2016; Polack et al., 2013; Reimer et al., 2014). Locomotion, in particular, has been found to
126 influence the activity of VIP- and SST-INs in a context-dependent manner, with the modulation of
127 SST-INs being contingent on the presence or absence of ambient light (Dipoppa et al., 2018;
128 Pakan et al., 2016). Whether such modulation by locomotion extends to other sensory cortices
129 remains unclear. In S1, behavioral periods associated with increased whisking (in stationary
130 animals) have been reported to increase L2/3 VIP- activity with concomitant decrease in L2/3
131 SST-INs firing in agreement with the presence of disinhibitory circuits (Gasselin et al., 2021;
132 Gentet et al., 2012; Lee et al., 2013; Muñoz et al., 2017; Yu et al., 2019). Nevertheless, in S1,
133 and in stark contrast to V1, our knowledge regarding the impact of locomotion on the operation of

134 SST- and VIP-INs remains limited. This becomes especially relevant considering that, during
135 navigation, mice typically employ locomotion in conjunction with whisking to explore their
136 surroundings.

137 Here we used intravital two-photon calcium imaging in S1 and V1 of awake, head-fixed
138 mice, to investigate how transitions in behavioral states (namely whisking and locomotion)
139 modulate the activity of SST- and VIP-INs, key disinhibitory elements of cortical networks. We
140 found that in darkness, the recruitment of SST-INs by locomotion was significantly higher in S1
141 than V1. We also observed that the increase of SST-INs activity in S1 occurred despite the strong
142 recruitment of VIP-INs, a known inhibitor of SST-INs. In addition, neither the strength of inhibition
143 provided by VIP-INs nor the sensitivity of SST-INs to cholinergic signaling was different across
144 sensory regions. Importantly, inactivation of thalamic function using muscimol microinjections
145 limited the increase in activity of SST-INs by locomotion. These results reveal that behavior state-
146 transitions, often associated with changes in arousal, induce sensory modality specific changes
147 to the activity of inhibitory circuits, most likely through inputs coming from the sensory thalamus.
148 By integrating feedforward thalamic activity transmitted indirectly via L2/3 PNs as well as
149 neuromodulatory information coming from VIP-mediated inhibition and cholinergic innervation,
150 SST-INs occupy a pivotal position in cortical networks by adapting sensory processing to
151 behavioral states in a sensory modality-specific manner.
152

153 **Results:**
154
155 *Activity of L2/3 SST-INs in S1 and V1 during spontaneous behavior*

156 We initially focused our attention on the *vivo* response of SST-INs to behavioral state
157 transitions in the mouse primary somatosensory cortex (S1). In fact, multiple studies have studied
158 the activity of disinhibitory circuits during active behavioral states in V1. However, it remains
159 unclear whether inhibitory circuits display similar or variable sensitivity to behavior state
160 transitions in other sensory cortical areas including S1. To monitor alterations in firing dynamics
161 of SST-INs we expressed the genetically encoded calcium indicator GCaMP6s selectively in SST-
162 IN using transgenic mice (SST-cre) (Figure 1A) and changes in somatic fluorescence of
163 GCaMP6s were used as a proxy for spiking activity. Fluorescence signals were recorded using
164 two-photon imaging in awake head fixed mice that spontaneously transitioned between rest and
165 locomoting periods on a circular treadmill (Figure 1A). Whisking activity was simultaneously
166 acquired using a video camera focused on the mouse snout (Figure 1A). This experimental setup
167 allowed us to study how SST-INs activity varied across active behavioral states namely during
168 whisking with and without associated running.

169 In our initial analysis, we categorized recording periods based on whether animals were
170 engaged in whisking, locomotion, or neither. Periods during which whisking or locomotion were
171 not detected were classified as resting (see Methods). Through the quantification of average
172 GCaMP6s fluorescence levels we found that in S1, SST-INs displayed markedly higher activity
173 levels during periods of locomotion compared to resting ($\Delta F/F_{0\ rest}$ = 0.80 ± 0.02; $\Delta F/F_{0\ run}$ = 1.84
174 ± 0.06; n = 2030 cells in 10 mice, $p<0.0001$, Mann-Whitney U test, Figure 1A-C). This engagement
175 of SST-INs during locomotion in S1 was also observed when we investigated the variability in the
176 response to behavior state transitions at the single cell level. For that we quantified the correlation
177 between baseline activity and running speed for individual SST-INs (Figure 1D). We observed a
178 predominantly positive correlation coefficient across SST-INs in S1 (Pearson correlation, ρ = 0.22
179 ± 0.01, n = 2030, Figure 1D). Specifically, 59% of SST-INs exhibited a statistically significant (see

methods) positive modulation in response to locomotion, while only a smaller but not negligible fraction of SST-INs displayed a significant negative modulation (20%) (Figure 1E)

These results contrasted with previous reports in V1, where in darkness, locomotion had on average, no impact in SST-INs activity (Dipoppa et al., 2018; Pakan et al., 2016). In order to test if this functional difference was linked to our experimental conditions or if in fact reflected a previously unknown region-specific modulation of SST-INs by locomotion we repeated the experiments listed above but now monitoring SST-INs activity in V1 (Figure 1E). In agreement with previous studies we observed that the modulation of SST-INs by locomotion in the dark in V1 was quite modest ($\Delta F/F_{0\ rest}$ = 0.70 ± 0.03; $\Delta F/F_{0\ run}$ = 0.84 ± 0.03; n = 881 cells in 10 mice, $p<0.0001$, Mann-Whitney U; (Dipoppa et al., 2018; Pakan et al., 2016) (Figure 1E,F) contrasting the results obtained in S1. This difference in activity of SST-INs during locomotion between S1 and V1 was also observed at the single cell level. In contrast to S1, our observations in V1 revealed a comparable ratio of SST-INs exhibiting positive (33%) and negative (25%) correlations between running speed and spontaneous activity (Figure 1G).

In order to better estimate the rate of change in calcium levels in SST-INs between S1 and V1 we generated population averages of all running or whisking bouts aligned to locomotion or whisking onset respectively (Figure 1H, I). In these population averages it was possible to observe that both locomotion as well as whisking induced changes in $\Delta F/F0$ in SST-INs that were significantly larger in S1 than in V1 (Figure 1J, I). The differential sensitivity of SST-INs between the two sensory areas to behavioral state transitions was particularly evident when comparing the cross-correlation curves between spontaneous activity of SST-INs and the locomotion or whisking traces (Pearson correlation: locomotion, S1, ρ = 0.20 ± 0.01, n=2030; V1, ρ = 0.05 ± 0.01, n=633; whisking, S1, ρ = 0.15 ± 0.01, n=853; V1, ρ = 0.04 ± 0.01, n=633, Figure 1K). Altogether these results suggest that in the neocortex, behavior-dependent modulation of SST-INs activity is not uniform across sensory regions.

206 *Contribution of whisking and locomotion to SST-INs modulation in S1*

207 Our results indicate that in S1 active behaviors like whisking and locomotion, result in
208 increased activity of SST-INs. However locomotion in mice is closely linked to the motion of their
209 whiskers (Mitchinson et al., 2007). In contrast, whisking can take place in both run and rest
210 conditions. We thus decided to further investigate how the two different active states (whisking
211 and locomotion) impacted the activity of SST-INs. In our experimental conditions mice were
212 observed to spend an average of 32% of their time running, 47% whisking, and within this
213 whisking period, 16% did not involve associated ambulatory activity (see Methods) (Figure 2A-B).
214 To facilitate a more straightforward comparison on how whisking and locomotion shaped activity
215 in SST-INs in S1 we specifically isolated recording periods in which mice were engaged in active
216 whisking without simultaneous running (Figure 2C-E). Under these conditions, which we defined
217 as "whisking only," the activity of SST-INs exhibited distinct differences compared to whisking
218 episodes that were accompanied by locomotion. Specifically, SST-INs were not positively
219 modulated during active whisking showing in contrast a tendency towards inhibition in agreement
220 with previous works (Gasselin et al., 2021; Gentet et al., 2012; Lee et al., 2013; Muñoz et al.,
221 2017) (Figure 2C-E). To further quantify how the different behavioral states influenced SST-INs
222 activity we separated calcium activity and we defined whisking only modulation index (WOMI) and
223 whisking modulation index (WMI) similar to our previous LMI calculation (see Methods). We
224 observed that both WMI and LMI were clearly positive and rather similar in agreement with the
225 observation that in mice most whisking bouts are actually associated with locomotion (Sofroniew
226 et al., 2014). In contrast WOMI, was only slightly positive with a large percentage of cells
227 displaying negative modulation (Figure 2F).

228 During our imaging sessions, we observed significant variation among mice in terms of
229 the duration of whisking without concurrent locomotion (% time WO = 15.6 ± 1.7%, CV = 105%,
230 n = 86 sessions). In light of this observation, we embarked on investigating whether the response
231 profile of SST-INs differed between sessions characterized by high or low percentages of WO.

232 Our rationale was that sessions with a higher proportion of WO activity would provide a better
233 opportunity to sample and visualize the specific impact of whisking with and without associated
234 locomotion. To achieve this, we employed an arbitrary threshold of 20% to categorize imaging
235 sessions into those with high or low percentages of WO (Figure 2G, H). We subsequently
236 identified all whisking bouts and averaged corresponding variations in GCaMP6s fluorescence
237 across the two different groups of sessions aligned to whisking onset. Upon examination of the
238 population's average response, distinct variations in the response of SST-INs to whisking became
239 evident between the two types of sessions (Figure 2G, H). In sessions with a high percentage of
240 whisking only, whisking onset was associated with a clear decrease in the activity of SST-INs
241 immediately after whisking onset. In contrast, in sessions where mice spent only a small fraction
242 of their time whisking without locomotion, whisking onset was clearly associated with an increase
243 in SST-INs firing (Figure 2G-H). Overall, these results indicate that in S1, whisking at rest induces
244 a decrease in SST-INs activity, in agreement with previous reports (Gentet et al., 2012; Muñoz et
245 al., 2017; Yu et al., 2019). On the other hand, when mice engage in active behavioral states
246 involving locomotion, activity of somatostatin interneurons (SST-INs) is increased, specifically in
247 the primary somatosensory cortex (S1), but not in the primary visual cortex (V1; Fig. 1). These
248 findings suggest that distinct active behavioral states exert varying effects on the activity of S1
249 SST-INs.

250 Morphoelectric and transcriptomic analysis have highlighted that SST-INs, even within
251 L2/3, are a highly heterogeneous neuronal population (Gouwens et al., 2020; Wu et al., 2023).
252 We probed if sensitivity to locomotion was also heterogeneous across individual SST-INs in S1.
253 To evaluate this, we separated SST-INs according to their response to WOMI. We observed that
254 SST-INs that displayed a negative WOMI, were on average less sensitive to locomotion (Figure
255 2I). In contrast, SST-INs with positive WOMI mostly increase their activity with locomotion (Figure
256 2I). Variable modulation of SST-INs for locomotion was observed even within single fields of view,
257 suggesting that variability in SST-IN responses cannot be attributed to distinct behavioral states

258 (Figure S1). In summary, these findings indicate the presence of various subtypes of SST-INs in
259 Layer 2/3, exhibiting varying degrees of sensitivity to transitions in behavioral states.
260
261 *VIP-INs are equally engaged by locomotion in V1 and S1*
262 Having observed that in S1, SST-INs are recruited during active behavioral states,
263 specifically during locomotion, we proceeded to investigate the underlying neuronal mechanisms
264 involved in such modulation. Taking into account previous works we identified three main potential
265 pathways that could participate in controlling L2/3 SST-INs activity during spontaneous behaviors:
266 (i) inhibitory top-down modulation via VIP-INs (Fu et al., 2014; Lee et al., 2013; Pfeffer et al., 2013;
267 Pi et al., 2013) (ii) increased local recurrent excitatory L2/3 PNs activity (Nestvogel and
268 McCormick, 2022; Pakan et al., 2016) and (iii) direct excitatory neuromodulation (*e.g.* via direct
269 cholinergic inputs) (Yaeger et al., 2019). We initially focused on VIP-INs, which are known to be
270 important inhibitors of SST-IN function (Fu et al., 2014; Lee et al., 2013; Pfeffer et al., 2013; Pi et
271 al., 2013) and are strong recipients of neuromodulatory inputs (*e.g.* cholinergic) associated with
272 active behavioral states (Alitto and Dan, 2013; Gasselin et al., 2021). Additionally, theoretical work
273 suggested that VIP-INs activation in certain conditions can result in unexpected increase in SST-
274 INs function through disinhibition of local PNs (Garcia Del Molino et al., 2017). Therefore, we
275 studied the contribution of VIP-INs to the activity patterns of SST-INs during behavioral state
276 transitions. We also explored the possibility that differential activity/function of VIP-INs could be
277 at the origin of the distinct sensitivity of SST-INs in V1 and S1 to locomotion.
278 We started by examining how activity of VIP-INs varied in S1 during the same behavioral
279 transitions as we described for SST-INs (Figure 3A-C). In line with previous findings (Fu et al.,
280 2015, 2014), we observed an increase in activity of VIP-INs during ambulatory periods in S1
281 ($\Delta F/F_{0\ rest}$ = 0.79 ± 0.02; $\Delta F/F_{0\ run}$ = 2.23 ± 0.05; n = 1915 cells; in 10 mice, $p<0.0001$, Mann-
282 Whitney U, Figure 3A, B, D) with the majority of VIP-INs displaying a positive modulation by
283 locomotion (LMI = 0.38 ± 0.01; Figure 3E). A similar observation was obtained while estimating

284 Pearson correlation between GCaMP6f or GCaMP6s fluorescence and running speed. VIP-INs
285 displayed on average a positive correlation ($\rho = 0.30 \pm 0.01$, Figure 3F) with only a very small
286 fraction (6%) of VIP-INs displaying a statistically significant decrease in activity (Figure 3F) during
287 locomotion. It is worth mentioning that the percentage of VIP-INs displaying negative modulation
288 by locomotion was significantly less than SST-INs (see Figure 1). Despite the similar average
289 positive modulation by locomotion between VIP- and SST-INs in S1, we observe that at the
290 population level, VIP-INs displayed a higher sensitivity to behavioral state transitions than SST-
291 INs (Figure S2). This was reflected into a higher correlation coefficient between spontaneous
292 activity and running speed (VIP: $\rho = 0.30 \pm 0.01$ vs SST: 0.22 ± 0.01, $p < 0.001$, Mann-Whitney U)
293 (Figure S1A) and different response profile between running speed and the variation in $\Delta F/F$ when
294 compared with SST-INs (Figure S2B). Similar findings were observed when analyzing whisking
295 only periods. In contrast to SST-INs, we observed that whisking only was associated with a clear
296 positive increase in the activity of VIP-INs in S1 (Figure S2C,D). This increased sensitivity of VIP-
297 INs to active states is likely explained by the enrichment of VIP-INs in nicotinic cholinergic
298 receptors when compared to SST-INs (Figure S2E, F and (Gasselin et al., 2021)).
299 Importantly, and in contrast to SST-INs we observed comparable modulation of VIP-INs
300 by locomotion in V1 and S1 (Figure 3C, G-I) (Pakan et al., 2016). Analogous findings were
301 obtained while studying whisking periods. We further investigated a potential difference in the
302 strength of inhibition from VIP-INs to SST-INs between the two primary sensory regions using ex-
303 vivo whole-cell patch-clamp recording. For that we used animals that expressed the Cre
304 Recombinase in VIP-INs while the FLP recombinase was expressed in SST-INs (Figure 3J). Such
305 transgenic mice allowed us to selectively express channelrhodopsin (ChR2) in VIP-INs and to
306 record light-evoked IPSCs from fluorescently labeled SST-INs (Figure 3J). We normalized
307 responses through comparison to simultaneously patched neighboring PNs. As previously
308 reported, we observed that VIP-mediated inhibition was higher in SST-INs when compared to
309 local PNs, but that this ratio was similar between S1 and V1 (Figure 3K). Taken together, our

310 findings indicate that changes in VIP-IN-mediated inhibition are likely not responsible for the
311 differential impact of locomotion and whisking in SST-INs between V1 and S1. In contrast, VIP-
312 INs are active during similar behavior periods as SST-INs in S1 suggesting possible functional
313 interactions during active states.
314
315 *VIP-INs inhibit SST-INs during active states in S1.*
316 In agreement with the classical "disinhibitory" scenario (Pfeffer et al., 2013), the activation
317 of VIP-INs is expected to decrease the activity of SST-INs. Our observation that during rest/run
318 transitions both VIP- and SST-INs in S1 increase their activity is not easy to reconcile with such
319 a hypothesis. Modeling studies raised the hypothesis that such as disinhibition of local PNs by
320 VIP-INs activation can be responsible for a simultaneous increase in VIP- and SST-INs firing
321 during active states (Garcia Del Molino et al., 2017). Hence, we performed experiments to assess
322 the influence of manipulating VIP-INs activity on the recruitment of SST-INs during active
323 behaviors in S1.
324 To achieve this, we used VIP-Cre::SST-Flp transgenic mice to express the inhibitory
325 DREADD hM4Di in VIP-INs while GCaMP6s was selectively expressed in SST-INs (Figure 4A-
326 B). Mice were initially imaged under control conditions, and then re-imaged 30 minutes after the
327 injection of CNO (1-10mg/Kg) to monitor potential changes in the activity of SST-INs (Figure 4B).
328 In both control conditions and after CNO injection, we observed an increase in average activity of
329 SST-INs during locomotion (control: $\Delta F/F_{0\ rest} = 0.71 \pm 0.04$; $\Delta F/F_{0\ run} = 1.52 \pm 0.07$; n = 393; Run:
330 $\Delta F/F_{0\ rest} = 0.61 \pm 0.04$; $\Delta F/F_{0\ run} = 1.81 \pm 0.08$; n = 308 cells in 5 mice, $p<0.0001$, Mann-Whitney
331 U) (Figure 4C). Interestingly, when investigating the modulation at the single cell level, we found
332 that SST-INs exhibited greater sensitivity to locomotion, as evidenced by elevated LMI and
333 Pearson correlation values (LMI: control = 0.30 ± 0.02, n = 393, CNO = 0.40 ± 0.02, n = 308 cells,
334 $p<0.001$, Mann-Whitney U test; Pearson: control = 0.30 ± 0.02, n = 393 , CNO = 0.44 ± 0.02, n =
335 308 cells, $p<0.01$, Mann-Whitney U test) (Figure 4D). In control conditions the proportion of

336 negatively modulated cells was also reduced in CNO treated mice (Figure 4D). We subsequently
337 averaged activity over all whisking periods aligning for whisking onset (Figure 4E). In control
338 condition we observed that immediately after whisking there was a decrease in SST-INs activity
339 that progressively increased as locomotion speed increased (Figure 4E-F). In CNO treated
340 conditions, the inhibitory effect after whisking was absent and overall, there was a larger increase
341 in positive modulation of SST-INs by locomotion (Figure 4F-E). Detailed analysis in the variation
342 of SST-INs activity with running speed also revealed that after CNO treatment a similar speed
343 produced a larger increase in $\Delta F/F_0$ signal in SST-INs (Figure 4G, H). These results suggest that
344 during active states VIP-INs have an overall inhibitory action in SST-INs and raises the question
345 about the underlying mechanism responsible for the active recruitment of L2/3 SST-IN during
346 locomotor activity.
347
348 *Visual stimulation alters SST-INs activity during active states in V1 but not in S1.*
349 Based on our results, the elevation in SST-INs activity during locomotion is not primarily
350 driven by VIP-mediated disinhibition of PNs. Instead, our results suggest the involvement of
351 alternative mechanisms. Whisking as well as locomotion are known to increase activity of
352 neuromodulatory inputs, namely cholinergic axons in neocortical regions (e.g. (Reimer et al.,
353 2014)). Recent work in mice suggested that L2/3 SST-INs in V1 loose their responsiveness to
354 cholinergic signaling, which could potentially account for their decreased sensitivity to active
355 states (Yaeger et al., 2019) but see (Bugeon et al., 2022). We tested if cholinergic signaling in
356 SST-INs was different between V1 and S1, which could potentially explain our results. Using
357 carbachol, a general agonist of acetylcholine receptors, we observed both in V1 as well as S1 a
358 depolarization of SST-INs that was blocked by the muscarinic receptor antagonist atropine (Figure
359 S3). This finding suggests equal equipment in cholinergic signaling in SST-INs between the two
360 sensory areas.

361 We thus looked for alternative pathways that could explain the positive modulation of SST-
362 INs during active states in S1. Recent work revealed that thalamic function is essential for the
363 arousal/movement-related activation of PNs in V1 (Nestvogel and McCormick, 2022). Inspired by
364 those findings we tested if feedforward signals transmitted to the cortex are also at the origin of
365 the observed modulation of SST-INs by active behavioral states. Such a possibility could also
366 eventually explain the difference in the modulation of SST-INs in V1 and S1 in the dark. Previous
367 works have reported that SST-INs in V1, which display modest to no modulation by locomotion in
368 the dark (Dipoppa et al., 2018; Fu et al., 2014; Pakan et al., 2016), show increased activity during
369 active states when mice are facing a grey screen (Dipoppa et al., 2018; Pakan et al., 2016). These
370 results are compatible with the idea that increased activity of thalamic neurons contribute to
371 defining the magnitude or direction of modulation of cortical SST-INs to behavioral transitions in
372 a sensory modality specific manner. We thus investigated whether in our working conditions visual
373 stimulation which is expected to increase the activity of the feedforward pathways into V1 altered
374 the sensitivity of SST-INs to behavioral transitions from rest to run in both S1 and V1. To achieve
375 this, we monitored the activity of SST-INs in both V1 and S1 under two conditions: in the dark and
376 in front of a grey screen (Figure 5A). We assessed changes in activity for both VIP- and SST-INs
377 from rest/run transitions by measuring variations of LMI as well as the Pearson correlation
378 between spontaneous activity and running speed (Figure 5). Our observations revealed that VIP-
379 INs activity remains relatively constant between S1 and V1, regardless of the dark or grey screen
380 conditions (Figure 5A-D). In contrast, SST-INs in V1 displayed a significantly greater sensitivity to
381 locomotion when facing a grey screen. Interestingly, the modulation of SST-INs in S1 by
382 locomotion appeared to be relatively unaffected by the dark versus grey screen conditions (Figure
383 5A-D). Altogether our results thus suggest that activity of feedforward pathways are important for
384 sensitivity of SST-INs to behavior state transitions.
385
386

387 *Thalamic activity is required for the modulation of SST-INs by spontaneous behaviors.*

388 As visual stimuli altered sensitivity of SST-INs to locomotion in V1 but not S1 we reasoned
389 that most likely thalamic activity is required for the modulation of SST-INs by active behavioral
390 states. We raised the hypothesis that in the dark, whisking leads to an increase in the S1
391 associated thalamic nuclei function (Petty et al., 2021) that is subsequently relayed to S1 and
392 explains the sensitivity of SST-INs to locomotion in the dark but not in V1. To directly test this
393 hypothesis, we inactivated the VPM and POM with microinjections of the GABA(A) agonist
394 muscimol (0.5 mM) and monitored the effect in SST-INs during resting and active states. We first
395 validated that we were able to effectively inactivate the somatosensory thalamus. For that we
396 conducted *in vivo* calcium imaging experiments in S1 while monitoring activity of PNs as well as
397 SST-INs in response to whisker stimulation in control conditions and after muscimol injections in
398 the somatosensory thalamus (Figure 6). We observed that in control conditions whisker
399 stimulation induced a clear increase in the activity of both SST-INs and PNs (Figure 6A-C and
400 Figure S4). In contrast, after muscimol injection this increase was absent in both cell types (Figure
401 6A-C and Figure S4). These results confirmed the effectiveness of muscimol in reducing thalamic
402 activity. Subsequently, we monitored the modulation of SST-INs in S1 by whisking and locomotion
403 in control conditions and after thalamus inactivation (Figure D-E). Interestingly when we evaluated
404 response of SST-INs to both whisking and locomotion there was a clear modification of the
405 response. In muscimol conditions there was a significant decrease in the response of SST-INs
406 during locomotion (control: $\Delta F/F_{0\ rest}$ = 0.53 ± 0.01; $\Delta F/F_{0\ run}$ = 1.02 ± 0.03; n = 1657; Run: $\Delta F/F_{0}$
407 $_{rest}$ = 0.53 ± 0.02; $\Delta F/F_{0\ run}$ = 0.76 ± 0.04; n = 541 cells in 8 mice, p<0.0001, Mann-Whitney U).
408 This effect translated into a decreased LMI both at the single cell level as well as when comparing
409 average values across the difference tested mice (LMI single cells: control = 0.18 ± 0.01, n =
410 1657, muscimol = 0.09 ± 0.01, n =541, <0.0001, Mann-Whitney U; Figure 6H, I). The Pearson
411 correlation between spontaneous activity and running speed was also significantly reduced by
412 thalamus inactivation (Pearson single cells: control = 0.18 ± 0.01, n = 1657, muscimol = 0.14 ±

413 0.01, n =541, <0.01, Mann-Whitney U; Figure 6I). Plotting variation in ΔF/F vs running speed
414 revealed once more that in control conditions SST-INs activity increased with running speed and
415 that this increase is significantly reduced after muscimol injections (Figure 6J). Overall, our results
416 suggest that in S1, modulation of SST-INs by spontaneous behaviors requires thalamic activity.
417
418 *In S1 locomotion is associated with increased L2/3 pyramidal cell activity.*
419 SST-INs are most likely not contacted directly by thalamic inputs (Sermet et al., 2019) and
420 receive information indirectly via their important connectivity with L2/3 PNs. We thus monitored
421 the *in vivo* spiking activity of L2/3 in S1 during behavior state transitions namely running and
422 whisking in control conditions and after muscimol injections in the somatosensory thalamus
423 (Figure 7). Our observations revealed a significant rise in spiking activity among L2/3 principal
424 neurons (PNs) in S1 during the transition from rest to running (control: $\Delta F/F_{0\,rest}$ = 0.22 ± 0.01; $\Delta F/F_{0}$
425 $_{run}$= 0.80 ± 0.03; n = 1918; p <0.0001, Mann-Whitney U; Figure 7B, C)). At the population level, we
426 noted that 44% of the cells exhibited a statistically significant increase in activity, while only 20%
427 displayed a decrease (Figure 7A-C). In contrast, after muscimol injection in the thalamus this
428 average increase in activity was completely absent (Figure 7E-G). In fact, positive correlation
429 between locomotion and GCaMP6s fluorescence traces was lost upon thalamus inactivation
430 (control: Pearson: 0.11 ± 0.01: n = 1918; run= -0.07 ± 0.0`; n = 371; p <0.0001, Mann-Whitney U;
431 Figure 7F, G). These results are in agreement with what has recently been reported using
432 electrophysiological approaches in the primary visual cortex (Nestvogel and McCormick,
433 2022). Furthermore, the increase in average ΔF/F values during running periods in pyramidal
434 cells was also not present in cells where somatosensory thalamus was inactivated by muscimol
435 injection (control: $\Delta F/F_{0\,rest}$ = 0.27 ± 0.01; $\Delta F/F_{0\,run}$= 0.22 ± 0.02; n = 371; p <0.0001, Mann-Whitney
436 U; Figure 7F, G). Hence, the convergence of locomotion-induced modulation and susceptibility
437 to thalamic inactivation in L2/3 PNs, similar to what we observed for SST-INs, further supports

438 the hypothesis that SST-INs in S1 inherit the increased activity during active behavioral states
439 from L2/3 PNs.

440 *Strongly heterogeneous glutamatergic inputs to SST enable PN-drive despite an overall*
441 *weak connection strength*

442 Glutamatergic inputs from L2/3 PNs to SST-INs are extremely weak, displaying low initial
443 release probably that progressively increases with continuous activation due to robust synaptic
444 facilitation (Kapfer et al., 2007; Pala and Petersen, 2015; Rozov et al., 2001). How can such weak
445 synapses transmit the increase in activity regimes in L2/3 PNs associated with active behavioral
446 states to L2/3 SST-INs? To address this, we performed paired recording between L2/3 PNs and
447 SST-INs in S1 and evaluated the strength of the excitatory connections between pairs of
448 connected neurons (Figure 7H). We observed that the synaptic strength (amplitude of first EPSC)
449 was highly variable among connections with an overall reduced mean amplitude and displaying
450 pronounced short facilitation (mean = 32 ± 6 pA, median = 12.8 pA, CV = 137%, n = 50) (Figure
451 7I, J). Interestingly, we observed that a small fraction (32 %) of cells displayed large initial current
452 amplitudes (amplitude of first EPSC >30 pA). In a subset of connected pairs, we managed to
453 successfully establish a third connection and we compared the synaptic properties between the
454 two different presynaptic neurons into the same postsynaptic SST-IN (Figure 7K,
455 L). Unexpectedly we observed that there was a positive correlation between the amplitude of the
456 synaptic currents between the two presynaptic neurons. These results suggest that the variability
457 in synaptic strength is not randomly distributed across glutamatergic synaptic inputs innervating
458 SST-INs but is determined by the postsynaptic subtype of SST-IN (Figure 7M). Overall, these
459 results indicate that a subpopulation of SST-INs is expected to be particularly sensitive to
460 variations in the activity level of L2/3 PNs that occur during the behavioral transitions from rest
461 active states in S1 in line with our initial *in vivo* observations (see Figure 1).

462
463

464 **Discussion:**
465
466 Using in vivo two-photon calcium imaging in awake mice we observed that behavioral state
467 transitions do not equally affect the activity of L2/3 SST-INs across primary sensory regions.
468 Specifically, we noted that in dark conditions, locomotion led to an increased activity of SST-INs
469 in the S1 but had no effect in V1. Interestingly, when visual stimulation was present, this difference
470 was lost and transitions from rest to running now positively modulated SST-INs in both primary
471 sensory regions. Variable recruitment of VIP-INs does not seem to be at the origin of such
472 differential behavior-state dependent modulation of SST-INs between the two sensory regions. In
473 addition, using a chemogenetic approach we revealed that VIP-INs mainly inhibit SST-INs during
474 rest/run transitions and are not the source of positive modulation of SST-INs by locomotion. In
475 contrast, we observed that inactivation of somatosensory thalamus strongly reduces the
476 modulation of SST-INs in S1 by spontaneous behaviors. Altogether our results provide a detailed
477 description of the neuronal mechanisms at the origin of the differential modulation of VIP- and
478 SST-INs by behavior states in S1.

479 The responses of neurons in primary sensory neocortical regions to sensory stimuli are
480 influenced by behavioral states including, arousal level, whisking, attention, and locomotion
481 (Bennett et al., 2013; Iriki et al., 1996; McGinley et al., 2015b; Petersen and Crochet, 2013).
482 Disinhibitory circuits have been recognized as key players in mediating the neuromodulatory
483 effects of such behavioral state transitions in neocortical networks. Specifically, the activity of VIP-
484 and SST-INs is believed to allow gain control by behavioral state in the neocortex (Fu et al., 2015,
485 2014). In fact, previous studies in V1 revealed that, in the dark, VIP-INs are recruited during
486 locomotion while the activity of SST-INs remains unchanged (Dipoppa et al., 2018; Fu et al., 2014;
487 Pakan et al., 2016). Interestingly, our findings indicate that in S1, SST-INs are strongly recruited
488 by locomotion even in the absence of light. This result is unexpected given the inhibitory
489 connection between VIP-INs and SST-INs, as well as the established role of VIP-INs in inhibiting

490 SST-INs during whisking in stationary animals (Gasselin et al., 2021; Gentet et al., 2012; Lee et
491 al., 2013; Pfeffer et al., 2013; Pi et al., 2013). Interestingly, when we selected from our recording
492 sessions periods of whisking with no associated locomotion, we reproduced previous findings
493 observed in non-locomoting mice. Namely, whisking resulted in an increase of VIP-INs activity
494 and a decrease in recruitment of SST-INs (Gentet et al., 2012; Muñoz et al., 2017). Hence, our
495 observations indicate that whisking during rest or during locomotion are associated with distinct
496 cortical states, with the latter resulting in significantly stronger recruitment of SST-INs in S1.

497 Notwithstanding the multiple evidence that SST-INs are sensitive to behavioral state
498 transitions the neuronal mechanisms at the origin of such modulations are not obvious. In the S1,
499 whisking in stationary animals mainly inhibits SST-INs in layer 2/3 (Gentet et al., 2012; Muñoz et
500 al., 2017). Through the manipulation of VIP-INs function, Munoz and colleagues provided
501 compelling evidence for VIP-INs to be the source of SST-INs inhibition during whisking in awake
502 mice (Muñoz et al., 2017). Surprisingly, during such experiments, the authors observed a reversal
503 in the response of SST-INs. Inhibiting VIP-INs resulted in a transformation of the modulation into
504 a notable positive recruitment of SST-INs by whisking (Muñoz et al., 2017). This finding highlights
505 the pivotal role of VIP-INs in governing the activity of SST-INs during whisking. However, the
506 question that emerges concerns the source of excitation by whisking in L2/3 SST-INs when VIP-
507 INs are silenced. We hypothesized that the mechanisms underlying such positive modulation are
508 probably also at the origin of positive modulation by locomotion that we now observed in S1.
509 Interestingly, in L5 SST-INs, pharmacological block or genetic removal of muscarinic receptors
510 abolishes positive increase in SST-INs by whisking indicating that cholinergic inputs are likely to
511 participate in increased activity of SST-INs by whisking (Muñoz et al., 2017). However, if a similar
512 mechanism is present in L2/3 SST-INs is unknown. At odds with a possible cholinergic modulation
513 of L2/3 SST-INs during spontaneous behaviours, Yaeger and colleagues (Yaeger et al., 2019),
514 reported that in the V1 of adult mice (P>56), SST-INs lose their sensitivity to cholinergic

515 modulation. However, it is worth noting that Yaeger et al. mainly reported changes at the
516 suprathreshold level upon cholinergic receptor activation. Consistent with the notion that
517 cholinergic modulation of SST-INs is absent in adult mice, theoretical analysis yielded a
518 hypothesis proposing that VIP-INs, rather paradoxically, may be responsible for the increase in
519 SST-INs, a phenomenon termed "response reversal," achieved through the disinhibition of local
520 PNs (Garcia Del Molino et al., 2017).

521 Our observations reveal that inhibiting VIP-INs does not abolish the positive modulation
522 of SST-INs by locomotion; instead, it has the opposite effect, increasing the sensitivity of SST-
523 INs to transitions from rest to running. This suggests that positive recruitment of SST-INs involves
524 mechanisms independent of VIP-INs. Furthermore, we noted that despite relatively similar
525 recruitment of VIP-INs across sensory regions, SST-INs in S1 and V1 displayed different
526 response profiles to locomotion particularly in dark conditions. This result further argues that VIP-
527 INs are likely not the cause of SST-INs increase during locomotion in the neocortex. In contrast,
528 our experimental results illustrate that in the presence of visual stimulation modulation of SST-
529 INs by locomotion is altered in V1 but not in S1 suggesting that sensory region-specific
530 mechanisms are involved in such modulation.

531 Based on our current findings, we propose a new working model in which the positive
532 modulation of SST-INs activity across behavioral states relies on the interaction between thalamic
533 activity and neuromodulatory pathways, specifically cholinergic inputs. Our hypothesis is strongly
534 supported by our data, which demonstrates that inactivation of the thalamus significantly
535 diminishes the modulation of SST-INs in S1 by locomotion. We propose that the involvement of
536 thalamic activity partially explains the region-specific effects of spontaneous behaviors on SST-
537 INs due to different levels of ongoing sensory drive. Activity of thalamocortical VPM neurons, that
538 relay somatosensory information to S1, increases with whisking (Gutnisky et al., 2017; Poulet et
539 al., 2012; Urbain et al., 2015). While comparatively less explored, recent findings suggest a

540 notable upsurge in VPM activity also during locomotion (Huo et al., 2020). For the moment is
541 unclear if this representation of self-motion in VPM neurons is due to cortical inputs (Poulet et al.,
542 2012), neuromodulation (Petty et al., 2021) or proprioception (Severson et al., 2017).
543 Nonetheless, we anticipate that the combined effects of whisking and locomotion lead to an
544 overall increase in thalamic activity, which is subsequently transmitted to the neocortex.
545 Interestingly, our findings align with recent research indicating that depolarization of L2/3 principal
546 neurons (PNs) in V1 during locomotion is dependent on thalamic function (Nestvogel and
547 McCormick, 2022). In fact, we obtained similar results in our study (Figure 6). Under normal
548 conditions, locomotion leads to an overall increase in activity (positive LMI) in L2/3 PNs (Figure
549 7), and this increase is entirely abolished when thalamic activity is disrupted. As SST-INs are
550 highly contacted by L2/3 PNs we suggest that the increase in SST-INs is inherited from L2/3 PNs.
551 Worth noting that in V1 the differential response of SST-INs to locomotion is also observed in L2/3
552 PN whose LMI is significantly larger in the present of visual stimulation (Pakan et al., 2016),
553 compatible with the idea that SST-INs display behavior dependent modulation in part transmitted
554 from local L2/3 PNs.

555 We also observed significant variability at the single-cell level regarding the sensitivity of
556 S1 L2/3 SST-INs to behavioral state transitions (see Figure 1 and 2). This variability was followed
557 by a pronounced variance in the strength of unitary connections between PNs and SST-INs
558 (Figure 7). Previous proposals have suggested that skewed distributions of excitatory
559 postsynaptic potential (EPSP) amplitudes in SST-INs, with a relatively small mean but a skew
560 towards larger amplitudes, ensured individual PNs to excite a subset of SST-INs (Kapfer et al.,
561 2007). However, our findings indicate that these distributions are not entirely random among SST-
562 INs and that the strength of these connections is influenced by the postsynaptic cell. Recent
563 transcriptomic data further suggest the presence of at least three distinct subtypes of SST-INs in
564 S1 L2/3 (Wu et al., 2023). Remarkably the expression of the Elfn1, which is known to retrogradely

565 regulate release dynamics at glutamatergic inputs, exhibits differential expression patterns among
566 SST-INs subtypes (Lim et al., 2018; Paul et al., 2017). This leads us to speculate that the
567 properties of glutamatergic inputs are not uniform across the different SST-IN subtypes in L2/3,
568 potentially conferring unique computational properties to neocortical circuits. In the future, it would
569 be interesting to directly investigate whether *in vivo* SST-INs exhibiting greater sensitivity to
570 locomotion correspond to those with stronger unitary connections between PNs and SST-INs that
571 we recorded *in vitro*. Subpopulations of SST-INs, with respect to their response during rest-run
572 transitions, were previously documented in V1 (Reimer et al., 2014). However, it remained
573 uncertain whether these responses genuinely corresponded to distinct subpopulations of SSTs
574 or if they were merely a result of transgenic mouse models used to label SST-INs (Hu et al.,
575 2013). In a more recent development, a study that employed a genetic approach to identify
576 subpopulations of SST-INs unveiled distinct functional specializations within these discrete
577 subsets of SST-INs (Green et al., 2023), further supporting the idea of the existence of SST-IN
578 subgroups.

579 During our thalamic muscimol injections, we observed a complete block of the positive
580 modulation of PNs by locomotion while it was only reduced in SST-INs. Since the experiments on
581 PNs and SST-INs were not conducted simultaneously, it remains possible that experimental
582 differences, such as incomplete thalamic inactivation during SST-INs imaging sessions, could
583 account for the disparate results despite ensuring successful targeting and delivery of muscimol
584 to the somatosensory thalamus. However, our in vitro results indicate that SST-INs are equipped
585 with cholinergic receptors. Thus, it is still possible that the remaining modulation of SST-INs is
586 mediated by cholinergic neuromodulation that remained active during our thalamus inactivation
587 experiment. Such a possible scenario would indicate that both thalamic and cholinergic pathways
588 are essential in shaping the responses of SST-INs in S1 across the different behavioral states.
589 Nonetheless, future work involving the selective removal of muscarinic receptors from SST-INs is

needed to allow definite claims about the in vivo contribution of cholinergic pathways in the control of L2/3 SST-INs during spontaneous behaviors.

Also evident was the observation that SST- and VIP-INs are equipped with different types of cholinergic receptors. VIP-INs were particularly rich in nicotinic receptors which were almost absent in SST-INs that seemed to express mainly muscarinic receptors. This differential equipment of cholinergic receptors is expected to result also in differential sensitivity to behavioral state transitions. In particular the high levels of nicotinic levels in VIP-INs are compatible with their fast activation to even small behavioral state variations like fast whisking bouts (Gasselin et al., 2021). In contrast for SST-INs, due to mainly muscarinic receptors, longer and more sustained activation of cholinergic inputs activation is required to mediate depolarizations in SST-INs.

Mechanistically it is now clear that both thalamus as well as neuromodulatory inputs like cholinergic projections originating from the basal forebrain participate in the modulation of cortical networks by behavioral state. Less obvious is the computational role of the two different pathways. The cholinergic pathway, via VIP-INs activation, has been proposed to underlie the gain control of L2/3 PNs to sensory evoked activity across behavioral states (Fu et al., 2014). Thalamic activity is required for the important depolarizations of L2/3 neurons (Nestvogel and McCormick, 2022) during locomotion but their precise computational role is still ill defined. In any case by integrating feedforward thalamic activity transmitted indirectly via L2/3 PNs as well as neuromodulatory information both via VIP-mediated inhibition and via direct cholinergic innervation, SST-INs occupy a key position in cortical networks to adjust activity of the two pathways and adjust neuronal activity in function of behavior state.

References:

Alitto, H., Dan, Y., 2013. Cell-type-specific modulation of neocortical activity by basal forebrain input. Front. Syst. Neurosci. 6.

Ayaz, A., Saleem, A.B., Schölvinck, M.L., Carandini, M., 2013. Locomotion controls spatial integration in mouse visual cortex. Curr. Biol. CB 23, 890–894. https://doi.org/10.1016/j.cub.2013.04.012

Bennett, C., Arroyo, S., Hestrin, S., 2013. Subthreshold Mechanisms Underlying State-Dependent Modulation of Visual Responses. Neuron 80, 350–357. https://doi.org/10.1016/j.neuron.2013.08.007

Bugeon, S., Duffield, J., Dipoppa, M., Ritoux, A., Prankerd, I., Nicoloutsopoulos, D., Orme, D., Shinn, M., Peng, H., Forrest, H., Viduolyte, A., Reddy, C.B., Isogai, Y., Carandini, M., Harris, K.D., 2022. A transcriptomic axis predicts state modulation of cortical interneurons. Nature 607, 330–338. https://doi.org/10.1038/s41586-022-04915-7

Busse, L., Cardin, J.A., Chiappe, M.E., Halassa, M.M., McGinley, M.J., Yamashita, T., Saleem, A.B., 2017. Sensation during Active Behaviors. J. Neurosci. 37, 10826–10834. https://doi.org/10.1523/JNEUROSCI.1828-17.2017

Dipoppa, M., Ranson, A., Krumin, M., Pachitariu, M., Carandini, M., Harris, K.D., 2018. Vision and Locomotion Shape the Interactions between Neuron Types in Mouse Visual Cortex. Neuron 98, 602-615.e8. https://doi.org/10.1016/j.neuron.2018.03.037

Fu, Y., Kaneko, M., Tang, Y., Alvarez-Buylla, A., Stryker, M.P., 2015. A cortical disinhibitory circuit for enhancing adult plasticity. eLife 4, e05558. https://doi.org/10.7554/eLife.05558

Fu, Y., Tucciarone, J.M., Espinosa, J.S., Sheng, N., Darcy, D.P., Nicoll, R.A., Huang, Z.J., Stryker, M.P., 2014. A cortical circuit for gain control by behavioral state. Cell 156, 1139–1152. https://doi.org/10.1016/j.cell.2014.01.050

Garcia Del Molino, L.C., Yang, G.R., Mejias, J.F., Wang, X.-J., 2017. Paradoxical response reversal of top-down modulation in cortical circuits with three interneuron types. eLife 6, e29742. https://doi.org/10.7554/eLife.29742

Gasselin, C., Hohl, B., Vernet, A., Crochet, S., Petersen, C.C.H., 2021. Cell-type-specific nicotinic input disinhibits mouse barrel cortex during active sensing. Neuron 109, 778-787.e3. https://doi.org/10.1016/j.neuron.2020.12.018

Gentet, L.J., Kremer, Y., Taniguchi, H., Huang, Z.J., Staiger, J.F., Petersen, C.C.H., 2012. Unique functional properties of somatostatin-expressing GABAergic neurons in mouse barrel cortex. Nat. Neurosci. 15, 607–612. https://doi.org/10.1038/nn.3051

Gouwens, N.W., Sorensen, S.A., Baftizadeh, F., Budzillo, A., Lee, B.R., Jarsky, T., Alfiler, L., Baker, K., Barkan, E., Berry, K., Bertagnolli, D., Bickley, K., Bomben, J., Braun, T., Brouner, K., Casper, T., Crichton, K., Daigle, T.L., Dalley, R., Frates, R.A. de, Dee, N., Desta, T., Lee, S.D., Dotson, N., Egdorf, T., Ellingwood, L., Enstrom, R., Esposito, L., Farrell, C., Feng, D., Fong, O., Gala, R., Gamlin, C., Gary, A., Glandon, A., Goldy, J., Gorham, M., Graybuck, L., Gu, H., Hadley, K., Hawrylycz, M.J., Henry, A.M., Hill, D., Hupp, M., Kebede, S., Kim, T.K., Kim, L., Kroll, M., Lee, C., Link, K.E., Mallory, M., Mann, R., Maxwell, M., McGraw, M., McMillen, D., Mukora, A., Ng, Lindsay, Ng, Lydia, Ngo, K., Nicovich, P.R., Oldre, A., Park, D., Peng, H., Penn, O., Pham, T., Pom, A., Popović, Z., Potekhina, L., Rajanbabu, R., Ransford, S., Reid, D., Rimorin, C., Robertson, M., Ronellenfitch, K., Ruiz, A., Sandman, D., Smith, K., Sulc, J., Sunkin, S.M., Szafer, A., Tieu, M., Torkelson, A., Trinh, J., Tung, H., Wakeman, W., Ward, K., Williams, G., Zhou, Z., Ting, J.T., Arkhipov, A., Sümbül, U., Lein, E.S., Koch, C., Yao, Z., Tasic, B., Berg, J., Murphy, G.J., Zeng, H., 2020. Integrated Morphoelectric and Transcriptomic Classification of Cortical GABAergic Cells. Cell 183, 935-953.e19. https://doi.org/10.1016/j.cell.2020.09.057

Green, J., Bruno, C.A., Traunmüller, L., Ding, J., Hrvatin, S., Wilson, D.E., Khodadad, T., Samuels, J., Greenberg, M.E., Harvey, C.D., 2023. A cell-type-specific error-correction signal in the posterior parietal cortex. Nature 620, 366–373. https://doi.org/10.1038/s41586-023-06357-1

Gutnisky, D.A., Yu, J., Hires, S.A., To, M.-S., Bale, M.R., Svoboda, K., Golomb, D., 2017. Mechanisms underlying a thalamocortical transformation during active tactile sensation. PLOS Comput. Biol. 13, e1005576. https://doi.org/10.1371/journal.pcbi.1005576

Hu, H., Cavendish, J., Agmon, A., 2013. Not all that glitters is gold: off-target recombination in the somatostatin–IRES-Cre mouse line labels a subset of fast-spiking interneurons. Front. Neural Circuits 7.

Huo, Y., Chen, H., Guo, Z.V., 2020. Mapping Functional Connectivity from the Dorsal Cortex to the Thalamus. Neuron 107, 1080-1094.e5. https://doi.org/10.1016/j.neuron.2020.06.038

Iriki, A., Tanaka, M., Iwamura, Y., 1996. Attention-induced neuronal activity in the monkey somatosensory cortex revealed by pupillometrics. Neurosci. Res. 25, 173–181. https://doi.org/10.1016/0168-0102(96)01043-7

Kapfer, C., Glickfeld, L.L., Atallah, B.V., Scanziani, M., 2007. Supralinear increase of recurrent inhibition during sparse activity in the somatosensory cortex. Nat. Neurosci. 10, 743–753. https://doi.org/10.1038/nn1909

Lee, S., Kruglikov, I., Huang, Z.J., Fishell, G., Rudy, B., 2013. A disinhibitory circuit mediates motor integration in the somatosensory cortex. Nat. Neurosci. 16, 1662–1670. https://doi.org/10.1038/nn.3544

Lim, L., Pakan, J.M.P., Selten, M.M., Marques-Smith, A., Llorca, A., Bae, S.E., Rochefort, N.L., Marín, O., 2018. Optimization of interneuron function by direct coupling of cell migration and axonal targeting. Nat. Neurosci. 21, 920–931. https://doi.org/10.1038/s41593-018-0162-9

McCormick, D.A., Nestvogel, D.B., He, B.J., 2020. Neuromodulation of Brain State and Behavior. Annu. Rev. Neurosci. 43, 391–415. https://doi.org/10.1146/annurev-neuro-100219-105424

McGinley, M.J., David, S.V., McCormick, D.A., 2015a. Cortical Membrane Potential Signature of Optimal States for Sensory Signal Detection. Neuron 87, 179–192. https://doi.org/10.1016/j.neuron.2015.05.038

McGinley, M.J., Vinck, M., Reimer, J., Batista-Brito, R., Zagha, E., Cadwell, C.R., Tolias, A.S., Cardin, J.A., McCormick, D.A., 2015b. Waking State: Rapid Variations Modulate Neural and Behavioral Responses. Neuron 87, 1143–1161. https://doi.org/10.1016/j.neuron.2015.09.012

Mitchinson, B., Martin, C.J., Grant, R.A., Prescott, T.J., 2007. Feedback control in active sensing: rat exploratory whisking is modulated by environmental contact. Proc. R. Soc. B Biol. Sci. https://doi.org/10.1098/rspb.2006.0347

Muñoz, W., Tremblay, R., Levenstein, D., Rudy, B., 2017. Layer-specific modulation of neocortical dendritic inhibition during active wakefulness. Science 355, 954–959. https://doi.org/10.1126/science.aag2599

Nestvogel, D.B., McCormick, D.A., 2022. Visual thalamocortical mechanisms of waking state-dependent activity and alpha oscillations. Neuron 110, 120-138.e4. https://doi.org/10.1016/j.neuron.2021.10.005

Niell, C.M., Stryker, M.P., 2010. Modulation of visual responses by behavioral state in mouse visual cortex. Neuron 65, 472–479. https://doi.org/10.1016/j.neuron.2010.01.033

Pakan, J.M., Lowe, S.C., Dylda, E., Keemink, S.W., Currie, S.P., Coutts, C.A., Rochefort, N.L., 2016. Behavioral-state modulation of inhibition is context-dependent and cell type specific in mouse visual cortex. eLife 5, e14985. https://doi.org/10.7554/eLife.14985

Pala, A., Petersen, C.C.H., 2015. In Vivo Measurement of Cell-Type-Specific Synaptic Connectivity and Synaptic Transmission in Layer 2/3 Mouse Barrel Cortex. Neuron 85, 68–75. https://doi.org/10.1016/j.neuron.2014.11.025

Paul, A., Crow, M., Raudales, R., He, M., Gillis, J., Huang, Z.J., 2017. Transcriptional Architecture of Synaptic Communication Delineates GABAergic Neuron Identity. Cell 171, 522-539.e20. https://doi.org/10.1016/j.cell.2017.08.032

Petersen, C.C.H., Crochet, S., 2013. Synaptic Computation and Sensory Processing in Neocortical Layer 2/3. Neuron 78, 28–48. https://doi.org/10.1016/j.neuron.2013.03.020

Petty, G.H., Kinnischtzke, A.K., Hong, Y.K., Bruno, R.M., 2021. Effects of arousal and movement on secondary somatosensory and visual thalamus. eLife 10, e67611. https://doi.org/10.7554/eLife.67611

Pfeffer, C.K., Xue, M., He, M., Huang, Z.J., Scanziani, M., 2013. Inhibition of inhibition in visual cortex: the logic of connections between molecularly distinct interneurons. Nat. Neurosci. 16, 1068–1076. https://doi.org/10.1038/nn.3446

Pi, H.-J., Hangya, B., Kvitsiani, D., Sanders, J.I., Huang, Z.J., Kepecs, A., 2013. Cortical interneurons that specialize in disinhibitory control. Nature 503, 521–524. https://doi.org/10.1038/nature12676

Polack, P.-O., Friedman, J., Golshani, P., 2013. Cellular mechanisms of brain state–dependent gain modulation in visual cortex. Nat. Neurosci. 16, 1331–1339. https://doi.org/10.1038/nn.3464

Poulet, J.F.A., Fernandez, L.M.J., Crochet, S., Petersen, C.C.H., 2012. Thalamic control of cortical states. Nat. Neurosci. 15, 370–372. https://doi.org/10.1038/nn.3035

Reimer, J., Froudarakis, E., Cadwell, C.R., Yatsenko, D., Denfield, G.H., Tolias, A.S., 2014. Pupil Fluctuations Track Fast Switching of Cortical States during Quiet Wakefulness. Neuron 84, 355–362. https://doi.org/10.1016/j.neuron.2014.09.033

Rozov, A., Burnashev, N., Sakmann, B., Neher, E., 2001. Transmitter release modulation by intracellular Ca2+ buffers in facilitating and depressing nerve terminals of pyramidal cells in layer 2/3 of the rat neocortex indicates a target cell-specific difference in presynaptic calcium dynamics. J. Physiol. 531, 807–826. https://doi.org/10.1111/j.1469-7793.2001.0807h.x

Saleem, A.B., Ayaz, A., Jeffery, K.J., Harris, K.D., Carandini, M., 2013. Integration of visual motion and locomotion in mouse visual cortex. Nat. Neurosci. 16, 1864–1869. https://doi.org/10.1038/nn.3567

Schneider, D.M., Nelson, A., Mooney, R., 2014. A synaptic and circuit basis for corollary discharge in the auditory cortex. Nature 513, 189–194. https://doi.org/10.1038/nature13724

Sermet, B.S., Truschow, P., Feyerabend, M., Mayrhofer, J.M., Oram, T.B., Yizhar, O., Staiger, J.F., Petersen, C.C., 2019. Pathway-, layer- and cell-type-specific thalamic input to mouse barrel cortex. eLife 8, e52665. https://doi.org/10.7554/eLife.52665

Severson, K.S., Xu, D., Van de Loo, M., Bai, L., Ginty, D.D., O'Connor, D.H., 2017. Active touch and self-motion encoding by Merkel cell-associated afferents. Neuron 94, 666-676.e9. https://doi.org/10.1016/j.neuron.2017.03.045

Shimaoka, D., Harris, K.D., Carandini, M., 2018. Effects of Arousal on Mouse Sensory Cortex Depend on Modality. Cell Rep. 22, 3160–3167. https://doi.org/10.1016/j.celrep.2018.02.092

Sofroniew, N.J., Cohen, J.D., Lee, A.K., Svoboda, K., 2014. Natural Whisker-Guided Behavior by Head-Fixed Mice in Tactile Virtual Reality. J. Neurosci. 34, 9537–9550. https://doi.org/10.1523/JNEUROSCI.0712-14.2014

Syeda, A., Zhong, L., Tung, R., Long, W., Pachitariu, M., Stringer, C., 2022. Facemap: a framework for modeling neural activity based on orofacial tracking. https://doi.org/10.1101/2022.11.03.515121

Urbain, N., Salin, P.A., Libourel, P.-A., Comte, J.-C., Gentet, L.J., Petersen, C.C.H., 2015. Whisking-Related Changes in Neuronal Firing and Membrane Potential Dynamics in the Somatosensory Thalamus of Awake Mice. Cell Rep. 13, 647–656. https://doi.org/10.1016/j.celrep.2015.09.029

Vinck, M., Batista-Brito, R., Knoblich, U., Cardin, J.A., 2015. Arousal and Locomotion Make Distinct Contributions to Cortical Activity Patterns and Visual Encoding. Neuron 86, 740–754. https://doi.org/10.1016/j.neuron.2015.03.028

Wu, S.J., Sevier, E., Dwivedi, D., Saldi, G.-A., Hairston, A., Yu, S., Abbott, L., Choi, D.H., Sherer, M., Qiu, Y., Shinde, A., Lenahan, M., Rizzo, D., Xu, Q., Barrera, I., Kumar, V., Marrero, G., Prönneke, A., Huang, S., Kullander, K., Stafford, D.A., Macosko, E., Chen, F., Rudy, B., Fishell, G., 2023. Cortical somatostatin interneuron subtypes form cell-type-specific circuits. Neuron 0. https://doi.org/10.1016/j.neuron.2023.05.032

Yaeger, C.E., Ringach, D.L., Trachtenberg, J.T., 2019. Neuromodulatory control of localized dendritic spiking in critical period cortex. Nature 567, 100–104. https://doi.org/10.1038/s41586-019-0963-3

Yu, J., Hu, H., Agmon, A., Svoboda, K., 2019. Recruitment of GABAergic Interneurons in the Barrel Cortex during Active Tactile Behavior. Neuron 104, 412-427.e4. https://doi.org/10.1016/j.neuron.2019.07.027

Zhou, M., Liang, F., Xiong, X.R., Li, L., Li, H., Xiao, Z., Tao, H.W., Zhang, L.I., 2014. Scaling down of balanced excitation and inhibition by active behavioral states in auditory cortex. Nat. Neurosci. 17, 841–850. https://doi.org/10.1038/nn.3701

Figure Legends

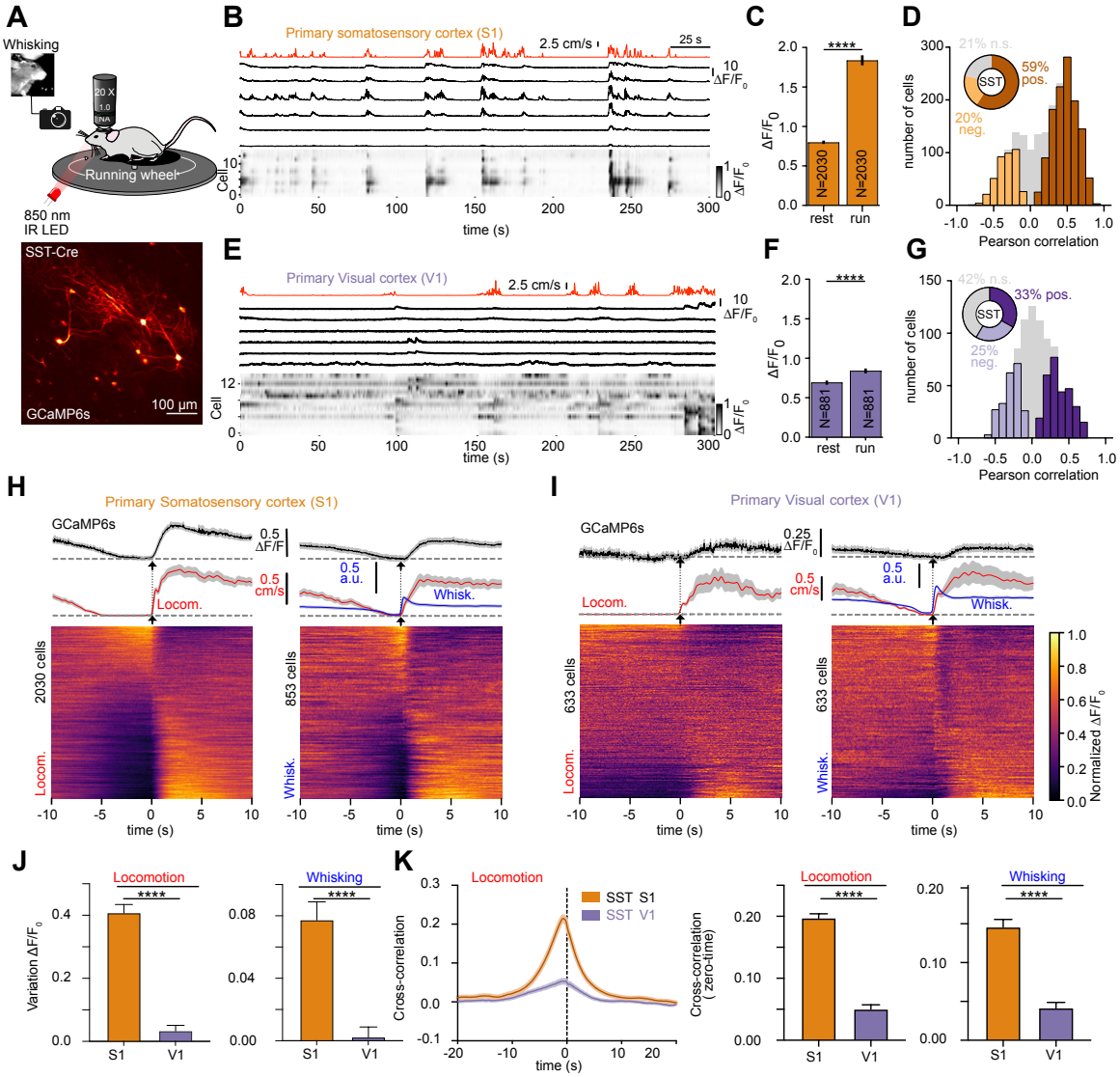

Figure 1: SST-INs in V1 and S1 are differentially modulated by behavioral state transitions. **(A)** Two-photon (2P) calcium imaging in S1 of awake mice. Mice were head fixed and were free to run on a circular treadmill. Whisking activity was tracked via a video camera detecting infra-red light focused on mouse snout illuminated with 850 nm LED. Bottom: Two-photon laser scanning microscopy (2PLSM) image (maximum-intensity projection, MIP) of SST-Cre positive neurons labelled with GCaMP6s in S1. Scale bar is 100 µm **(B)** Representative GCaMP6s fluorescence traces (black) shown as $\Delta F/F_0$ (up) as well as normalized $\Delta F/F_0$ (bottom) for SST-INs displayed in A. Each row represents a neuron sorted by weight on the first principal component (PC) of their activity. Locomotion trace is shown on top (red). **(C)** Mean $\Delta F/F_0$ during periods of rest and run ($\Delta F/F_{0\ rest}$ = 0.80 ± 0.02; $\Delta F/F_{0\ run}$ = 1.84 ± 0.06; n = 2030 cells in 16 mice, $p<0.0001$, Mann-Whitney U test). **(D)** Summary plot of Pearson correlation coefficients between calcium activity and running speed. SST-INs showing statistically significant (see methods) modulation by locomotion are represented by colored bars, with light orange indicating negative modulation and positive modulation denoted by brown. The pie chart provides an overview of the overall percentage of SST-INs showing positive, negative, or no effect in response to locomotion. **(E)** Same as B but for SST-INs in the primary visual cortex. (**F, G**) Same as C and D but for V1. $\Delta F/F_0$

$_{rest}$ = 0.70 ± 0.03; $\Delta F/F_{0\ run}$ = 0.84 ± 0.03; n = 881 cells in 10 mice, p<0.0001, Mann-Whitney U. **(H)** Event-triggered average traces of SST-INs GCaMP6s signal in S1 aligned to the start of running (left) or whisking (right) along with running speed (red) and whisking (blue). Normalized ΔF/F is displayed for all analyzed cells (bottom). Traces represent mean ± SEM values across all recorded cells. **(I)** Same as G but for V1. **(J)** Summary plot of variation in ΔF/F between rest and run and rest and whisking for the event-triggered average traces shown in G and H. Values were obtained by averaging ΔF/F trace for each individual SST-INs in a 2 s window before and after event onset (see Methods). $\Delta F/F_{0\ Loco\ S1}$ = 0.40 ± 0.03, n = 2030; $\Delta F/F_{0\ Loco\ V1}$ = 0.03 ± 0.02, n= 633, p<0.0001, Mann-Whitney U; $\Delta F/F_{0\ Whisk\ S1}$ = 0.08 ± 0.01, n = 853, n = 2030, $\Delta F/F_{0\ Whisk\ V1}$ = 0.002 ± 0.007; n = 853 cells in 10 mice, p<0.0001, Mann-Whitney U. **(K)** Cross-correlation between in vivo calcium activity and running speed for SST-INs in S1 and V1 (left). (right) Average correlation coefficient values at zero-time for locomotion and whisking for SST-INs recorded in V1 and S1 (ploco S1 = 0.22 ± 0.01, n = 2030, ploco V1 = 0.06 ± 0.01, n = 883, p<0.0001, Mann-Whitney U; pwhisk S1 = 0.15 ± 0.01, n = 2030, ploco V1 = 0.05 ± 0.01, n = 883, p<0.0001, Mann-Whitney U).

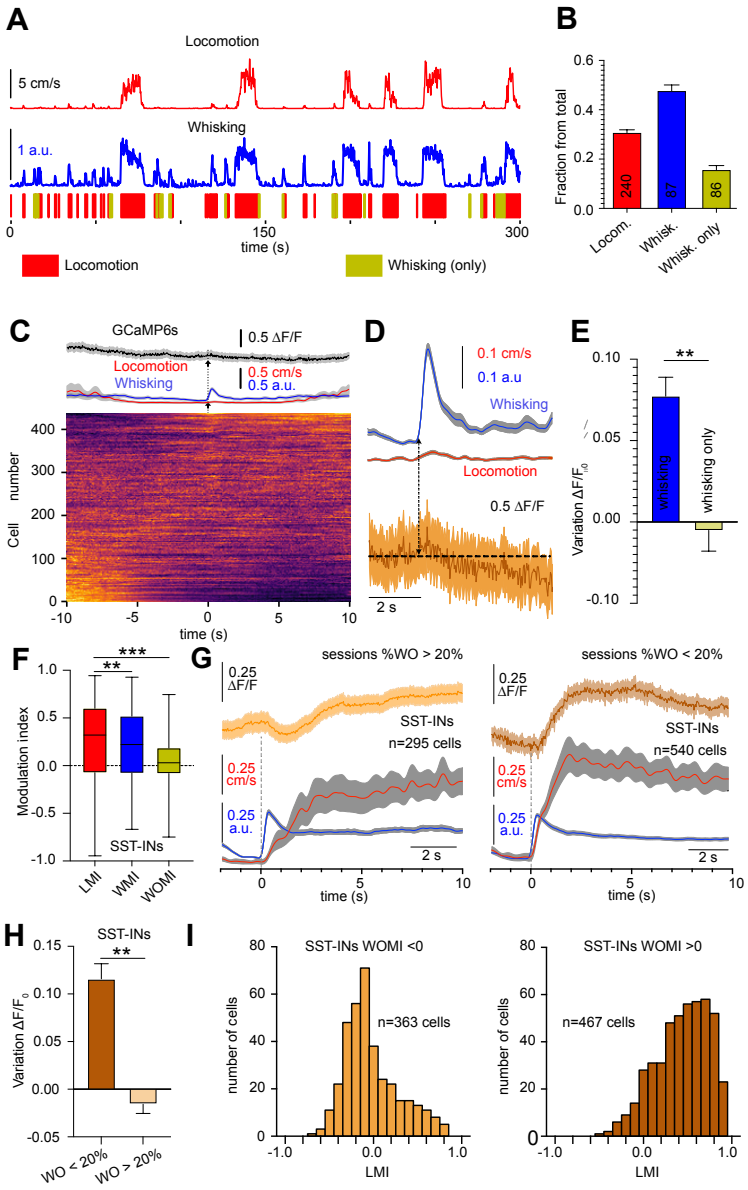

Figure 2: Recruitment of SST-INs in S1 is primarily associated with behavioral state transitions characterized by increased locomotor activity. (A) Example session illustrating simultaneous recording traces for whisking (blue) and running speed (red). Whisking only periods (no locomotor activity) are highlighted in light green. **(B)** Quantification of the fraction of time mice spent whisking, wishing only and running during imaging sessions. **(C)** Event-triggered average traces of SST-INs GCaMP6s fluorescence signal in S1 aligned to whisking onset. Only whisking bouts not associated with locomotion were used (whisking only). Normalized ΔF/F is displayed for all analyzed cells (bottom). Traces represent mean ± SEM values across all recorded cells. **(D)** Enlarged view of average traces shown in C. **(E)** Summary plot of variation in ΔF/F between rest and whisking for the event-triggered average traces shown in C and panel H figure1. Values were obtained by averaging ΔF/F traces for each individual SST-INs in a 2 s window before and after event onset. Note that during whisking only, there is either no effect or a slight tendency to inhibit SST-INs. However, when whisking is associated with running periods, it clearly increases the activity of SST-INs. $\Delta F/F_{0\ Whisk}$ = 0.08 ± 0.01, n = 853; $\Delta F/F_{0\ Whisk\ only}$ = -0.01 ± 0.01; n = 853

835 cells in 10 mice, $p<0.001$, Mann-Whitney U. **(F)** Summary plot of average mean locomotion,
836 whisking and whisking only modulation indices (LMI = 0.26 ± 0.01, n=2030; WMI = 0.21 ± 0.01,
837 n=856; WOMI = 0.06 ± 0.01, n=830) **(G)** Event-triggered average traces of SST-INs GCaMP6s
838 signal ($\Delta F/F$) in S1 aligned to whisking onset. Results were separated according to percentage
839 time mice spent whisking only during the imaging session. Average of GCaMP6s fluorescence
840 from sessions with whisking only periods longer than 20% of the recording time is shown on the
841 left and less than 20% is illustrated on the right. Traces represent mean ± SEM values across all
842 recorded cells. **(H)** Summary plot of variation in $\Delta F/F$ between rest and whisking for the event-
843 triggered average traces shown in G. Average values were obtained 2 s before and 2 s after event
844 whisking onset (see Methods). Values were calculated for each individual SST-INs. ($\Delta F/F_{0\ Whisk<20\%}$
845 = 0.11 ± 0.02, n = 602; $\Delta F/F_{0\ Whisk<20\%}$ = -0.02 ± 0.01, n = 251, $p<0.0001$, Mann-Whitney
846 U). **(I)** Histograms of the distribution of locomotion modulation indices (LMI = $(R_L - R_S)/(R_L + R_S)$,
847 where R_L and R_S are the mean $\Delta F/F0$ during locomotion and stationary periods, respectively), for
848 SST-INs that displayed negative or positive WOMI.
849

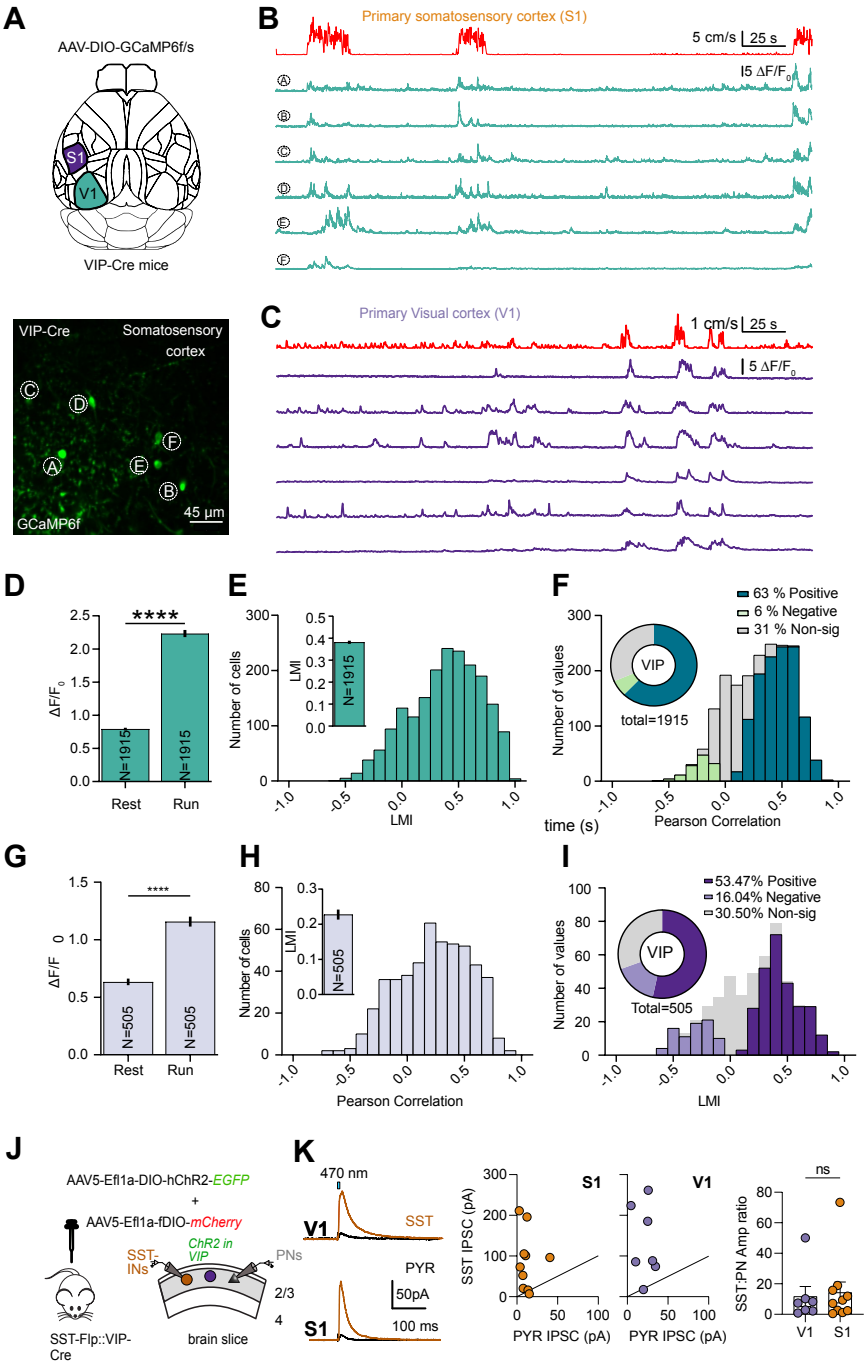

Figure 3: VIP interneurons are strongly modulated by locomotion in S1. A) *(top)* Illustration of a mouse brain depicting the location of S1 and V1. *(bottom)* 2PLSM image (maximum-intensity projection, MIP) of VIP-Cre positive neurons labeled with GCaMP6f in S1. **B)** Representative traces of in vivo calcium (GCaMP6f) activity in VIP-INs. Locomotion trace is shown on top (red) followed by the calcium activity (green). Deconvolved activity (in black) is shown under each trace **C)** Same as B but for VIP-INs in V1. **D)** Mean $\Delta F/F_0$ during periods of rest and run, ($\Delta F/F_{0\ rest}$ = 0.80 ± 0.02; $\Delta F/F_{0\ run}$ = 2.23 ± 0.05; n = 1915 cells in 11 mice, p<0.0001, Mann-Whitney U test). **E)** Histogram of locomotion modulation indices for VIP-INs in S1. Inset depicts the average LMI value (LMI = 0.38 ± 0.01, n= 1915). **F)** Distribution of Pearson correlation coefficients between

calcium activity and locomotion trace for VIP-INs in S1. Colored bars indicate VIP-INs that are statistically significantly modulated by locomotion, either in a negative (orange) or positive manner. The pie chart provides an overview of the overall percentage of VIP-INs showing positive, negative, or no effect in response to locomotion**. G, H , I)** Same as D, E, F but for VIP-INs in V1. **J)** Illustration of the double transgenic mouse line used for targeted protein expression in VIP- and SST-INs respectively. Adeno-associated virus (AAV) coding Cre-dependent expression of Channelrhodopsin2-EGFP along with a second AAV coding FLP-dependent expression of mCherry were infected in primary visual (V1) and primary sensory (S1) cortices of VIP-Cre::SST-Flp mice. Schematic diagram of experimental approach where VIP-INs were photo-activated via ChR2 while a PN and neighboring SST-IN were patched in L2/3. **K)** *(left)* Example traces of IPSCs simultaneously recorded in PNs and SST in V1 and S. *(middle)* Scatter plot of IPSCs amplitudes recorded in SST-INs and PNs in S1 and V1 following VIP-INs photostimulation. (*right*) Ratio of light-evoked IPSCs in V1 and S1 (V1: n = 7 cells, 2 mice ; S1: n = 10 cells, 2 mice). Mann Whitney test p=0.8125. Error bars represent SEM.

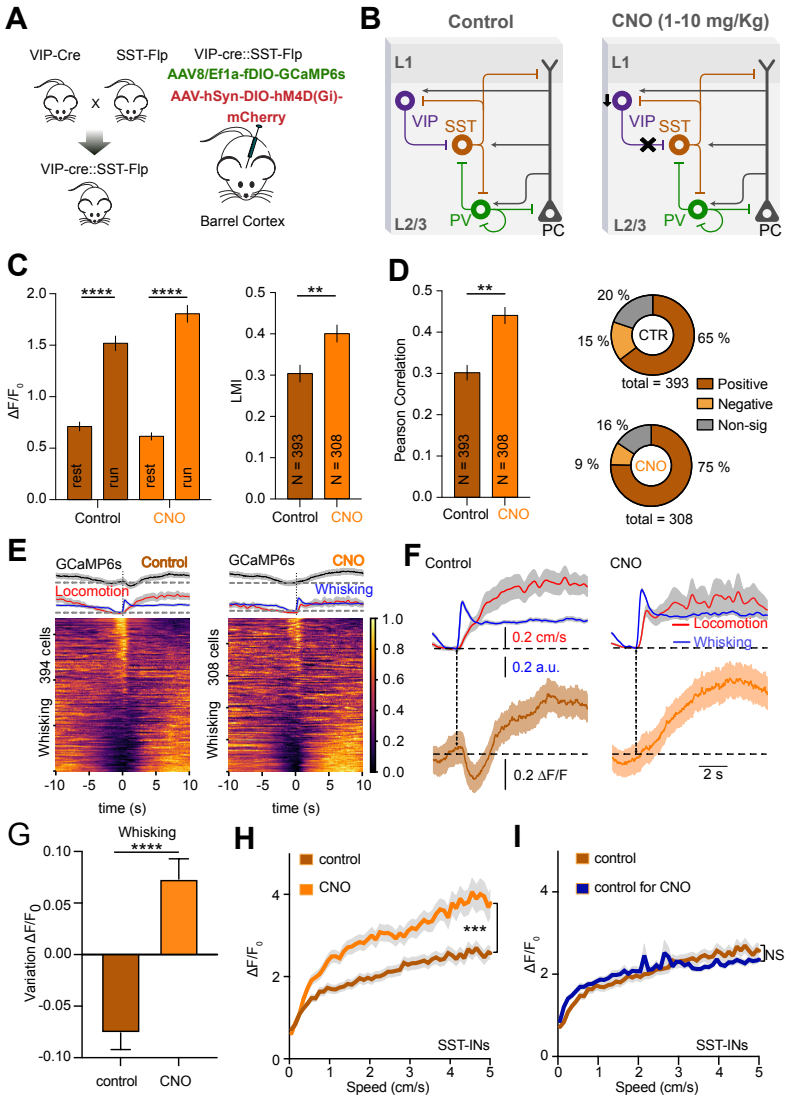

Figure 4:VIP-INs mainly inhibit SST-INs during spontaneous behaviors. A) Simplified illustration of the double transgenic mouse line used to target protein expression in VIP- and SST-INs respectively based on the Cre/Lox and FLP/FRT system. Adeno-associated viruses (AAV) were used to express in a Cre-dependent manner G_i-coupled inhibitory (hM4Di) designer receptors exclusively activated by designer drugs (DREADD) in VIP-INs. A second AAV was used to drive in a FLP-dependent manner the expression of GCaMP6s in SST-INs. **B)** Schematic illustration of the canonical cellular organization in S1 and the expected negative modulation of VIP-INs via activation of hM4Di by CNO injection. **C)** Mean $\Delta F/F_0$ during periods of rest and run in control conditions and 30 after CNO injection (left), ($\Delta F/F_{0\ rest,\ control} = 0.71 \pm 0.02$; $\Delta F/F_{0\ run,\ control} = 1.5 \pm 0.07$; n = 393 cells in 5 mice, $p<0.0001$, Mann-Whitney U test; $\Delta F/F_{0\ rest,\ CNO} = 0.61 \pm 0.04$; $\Delta F/F_{0\ run,\ CNO} = 1.81 \pm 0.08$; n = 308 cells in 5 mice, $p<0.0001$, Mann-Whitney U test). Summary plot of LMI values obtained for SST-INs in control and after CNO injection (right), (LMI control = 0.30 ± 0.02, n = 393; LMI CNO = 0.4 ± 0.02, n = 308; $p<0.001$, Mann-Whitney U test). **D)** Variation in Pearson correlation values between running speed and GCaMP6s fluorescence signals for SST-INs recorded in control and CNO treated mice (ρloco control = 0.30 ± 0.02, n = 393, ρloco CNO = 0.44 ± 0.02, n = 308, $p<0.0001$, Mann-Whitney U). Percentage of SST-INs exhibiting statistically significant positive, negative, or non-significant Pearson correlation values is shown

893 on the right. **E)** Event-triggered average traces of SST-INs GCaMP6s signals in S1 aligned to the
894 onset of whisking along with running speed (red) and whisking (blue). Normalized ΔF/F is
895 displayed for all analyzed cells (bottom). Results are displayed for control conditions (left) and
896 after CNO injection (right). Traces represent mean ± SEM values across all recorded cells. **F)**
897 Enlarged view of average traces shown in E. **G)** Summary plot of variation in ΔF/F between rest
898 and whisking for the event-triggered average traces shown in F. Average values were obtained 2
899 s before and 2 s after event whisking onset (see Methods). Values were calculated for each
900 individual SST-INs. Note that in control conditions whisking induces a brief decrease in GCaMP6s
901 fluorescence that is absent in CNO treated mice. **H and F)** Variation in ΔF/F values for SST-INs
902 with running speed for control and CNO conditions.
903

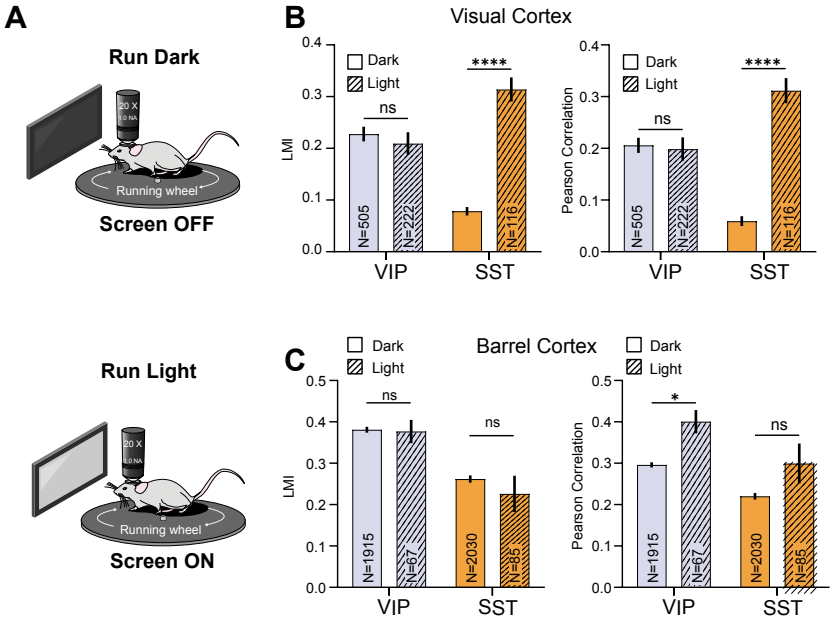

Figure 5: Visual stimulation modulates the recruitment of SST-INs by locomotion in V1 but not in S1. A) Schematic of the experimental setup used to probe the effect of visual stimulation in the behaviour state-dependent modulation of the activity of VIP and SST-INs in V1 and S1. **B)** Summary plots of LMI and Pearson correlation between running speed and GCaMP6 fluorescence signal for VIP- and SST-INs in the dark and facing a grey screen. LMI = 0.23 ± 0.01, n =505, for VIP in the dark versus 0.21 ± 0.02, n = 222, in light; p > 0.9999, and 0.08 ± 0.01, n = 881 for SST in the dark versus 0.31 ± 0.02, n = 116 in light, p < 0.0001. Pearson Correlation: 0.21 ± 0.01, n = 505, for VIP in the dark versus 0.20 ± 0.02, n = 222, in light; 0.06 ± 0.01, n = 881, for SST in the dark versus versus 0.31 ± 0.02, n = 116 for SST-INs in light, p < 0.0001, Mann-Whitney U test. **C)** Same as B but for S1. Values represent mean ± SEM.

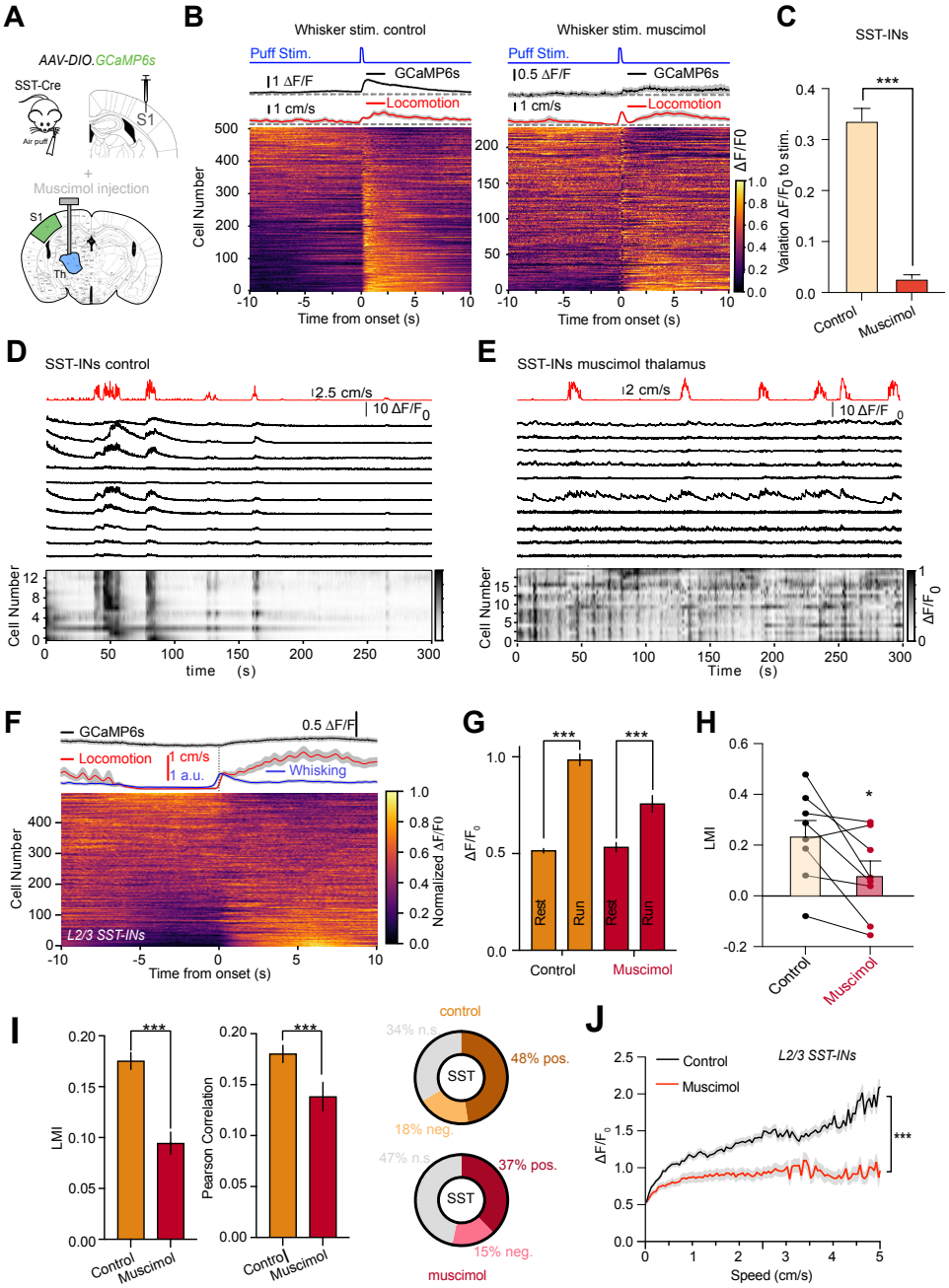

Figure 6: Thalamic activity is required for the modulation of SST-INs by locomotion in S1. A) Schematic illustration of experimental approach used to monitor effectiveness of thalamus inactivation using muscimol injection in somatosensory thalamus. Whisker deflection was achieved using localized air puff while cortical activity in S1 was monitored using *in vivo* two-photon calcium imaging. **B)** Event-triggered average traces of SST-INs GCaMP6s signals in S1 aligned to whisker puff along with running speed (red). Normalized ΔF/F is displayed for all analyzed cells (bottom). Results are displayed for control conditions (left) and for mice previously injected with muscimol in the thalamus (*right*). Traces represent mean ± SEM values across all recorded cells. **C)** Summary plot of variation in ΔF/F between rest and after whisker stimulation for the event-triggered average traces shown in B. Average values were obtained 2 s before and 2 s after whisker stimulation onset (see Methods). **D)** Representative GCaMP6s fluorescence

929 traces (black) shown as $\Delta F/F_0$ (up) as well as normalized $\Delta F/F_0$ (bottom) for SST-INs in S1 for
930 mice spontaneously transitioning between rest and active behavior periods. Each row represents
931 a neuron sorted by weight on the first principal component (PC) of their activity. Locomotion trace
932 is shown on top (red). **E)** Same as A but for mice treated with muscimol injection in the
933 somatosensory thalamus (VPM and POM). **F)** Event-triggered average traces of SST-INs
934 GCaMP6s signals in S1 aligned to the onset of locomotion along with running speed (red) and
935 whisking (blue). Normalized $\Delta F/F$ is displayed for all analyzed cells (bottom). Results are
936 displayed for mice previously injected with muscimol in the thalamus. Traces represent mean ±
937 SEM values across all recorded cells. **G)** Mean $\Delta F/F_0$ during periods of rest and run in control
938 conditions and 30 min microinjection of muscimol in the somatosensory thalamus ($\Delta F/F_{0\ rest\ control}$
939 = 0.53 ± 0.01; $\Delta F/F_{0\ run\ control}$ = 1.01 ± 0.03; n = 1657 cells in 8 mice, p<0.0001, Mann-Whitney U
940 test; $\Delta F/F_{0\ rest\ muscimol}$ = 0.53 ± 0.02; $\Delta F/F_{0\ run\ muscimol}$ = 0.76 ± 0.04; n = 541 cells in 8 mice, p<0.0001,
941 Mann-Whitney U test). **H)** Summary plot of average LMI obtained in control and after muscimol
942 injection per the different individual mice tested ($LMI_{control}$ = 0.23 ± 0.06, $LMI_{muscimol}$ = 0.08 ± 0.06,
943 n = 8 mice, p = 0.0391, Wilcoxon test. **I)** Summary plots for LMI (left) and Pearson correlation
944 values (middle) between running speed and calcium activity for SST-INs in S1 obtained in control
945 and after muscimol injection in the thalamus ($LMI_{control}$ = 0.18 ± 0.01, n = 1657, $LMI_{muscimol}$ = 0.10
946 ± 0.01, n = 541, p < 0.0001 Mann-Whitney U test; Pearson, $\rho_{control}$ = 0.18 ± 0.01, n = 1657, $\rho_{muscimol}$
947 = 0.14 ± 0.01, n = 541, p < 0.05 Mann-Whitney U test) . Percentage of SST-INs exhibiting
948 statistically significant positive, negative, or non-significant Pearson correlation values is shown
949 on the right. **J)** Variation in $\Delta F/F$ values for SST-INs with running speed for control and muscimol
950 injection conditions.
951

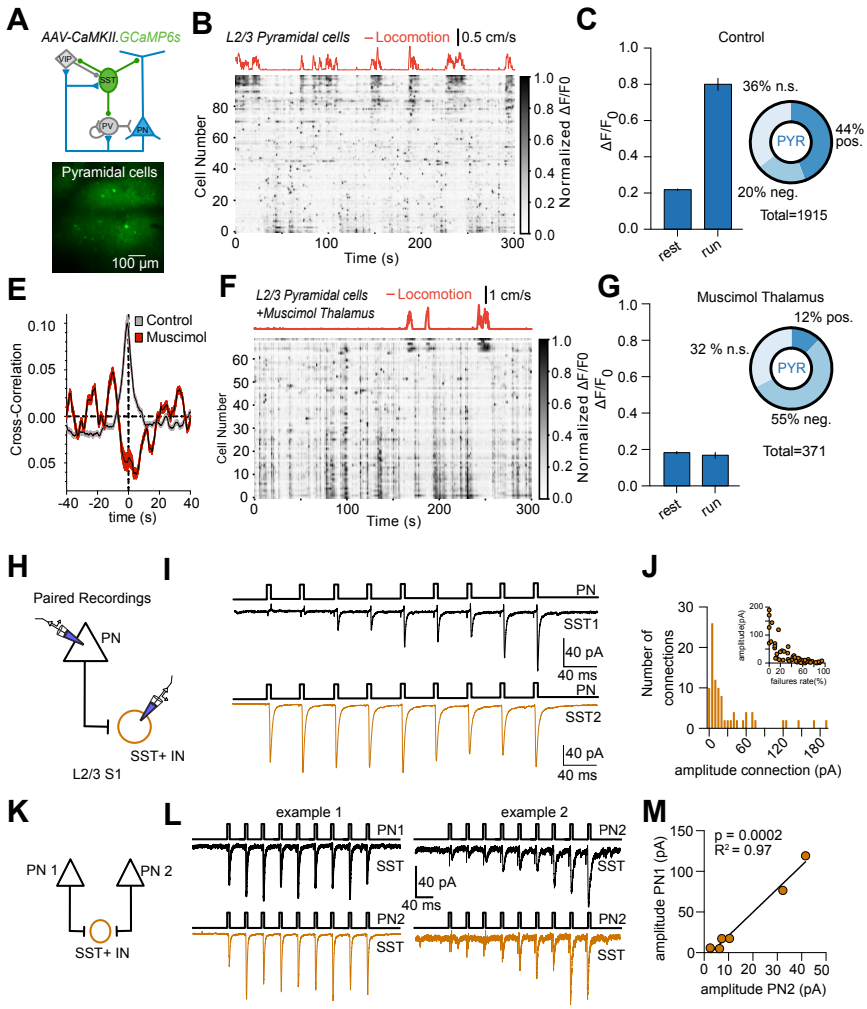

Figure 7: Behavioral state transitions from rest to active states increase activity of pyramidal cells in S1. A) Top: schematic illustration of layer 2/3 microcircuits in S1; bottom: in vivo 2PSLM images of S1 PNs labeled with GCaMP6s. **B)** Raster plot of the pyramidal cell activity in the S1 from awake mice spontaneously transitioning between resting periods and periods of locomotion. Each row represents a neuron sorted by weight on the first principal component (PC) of their activity. **C)** Mean $\Delta F/F_0$ during periods of rest and run (Control: $\Delta F/F_{0\ rest} = 0.21 \pm 0.01$; $\Delta F/F_{0\ run} = 0.80 \pm 0.04$; n = 1918 cells in 3 mice, $p<0.0001$, Mann-Whitney U test). **E)** Cross-correlation between in vivo calcium activity and running speed for Pyramidal neurons in S1 in control condition and after muscimol injections in somatosensory thalamus. **F-G)** Same as B and C but mice previously microinjected with muscimol in thalamus **(**Muscimol: $\Delta F/F_{0\ rest} = 0.18 \pm 0.01$; $\Delta F/F_{0\ run} = 0.17 \pm 0.16$; n = 371 cells in 2 mice, $p<0.0001$, Mann-Whitney U test). **H)** Schematic illustration of dual whole-cell patch clamp configuration used to record synaptic properties of unitary connections between individual L2/3 PNs and local SST-INs. **I)** Example traces of a train of EPSCs recorded from two different SST-INs in response to presynaptic action potential induction in two different L2/3 PNs. Note the pronounced different in the amplitude of the first EPSC between the two SST-INs. **J)** Histogram of amplitudes of first EPSC obtained for 50 synaptic unitary connections. Inset depicts the relationship between amplitude and failure rate for the 50 connections. **K)** Same as for **H** but illustrating that the properties of two different presynaptic L2/3 PNs were recorded for the same postsynaptic SST-INs. **L)** Example traces of EPSCs recorded in two different SST-INs for four presynaptic PNs. **M)** Summary plot indicating

973 the relationship between the amplitude obtained when stimulating PN1 or PN2 for the same
974 postsynaptic SST-INs.
975
976

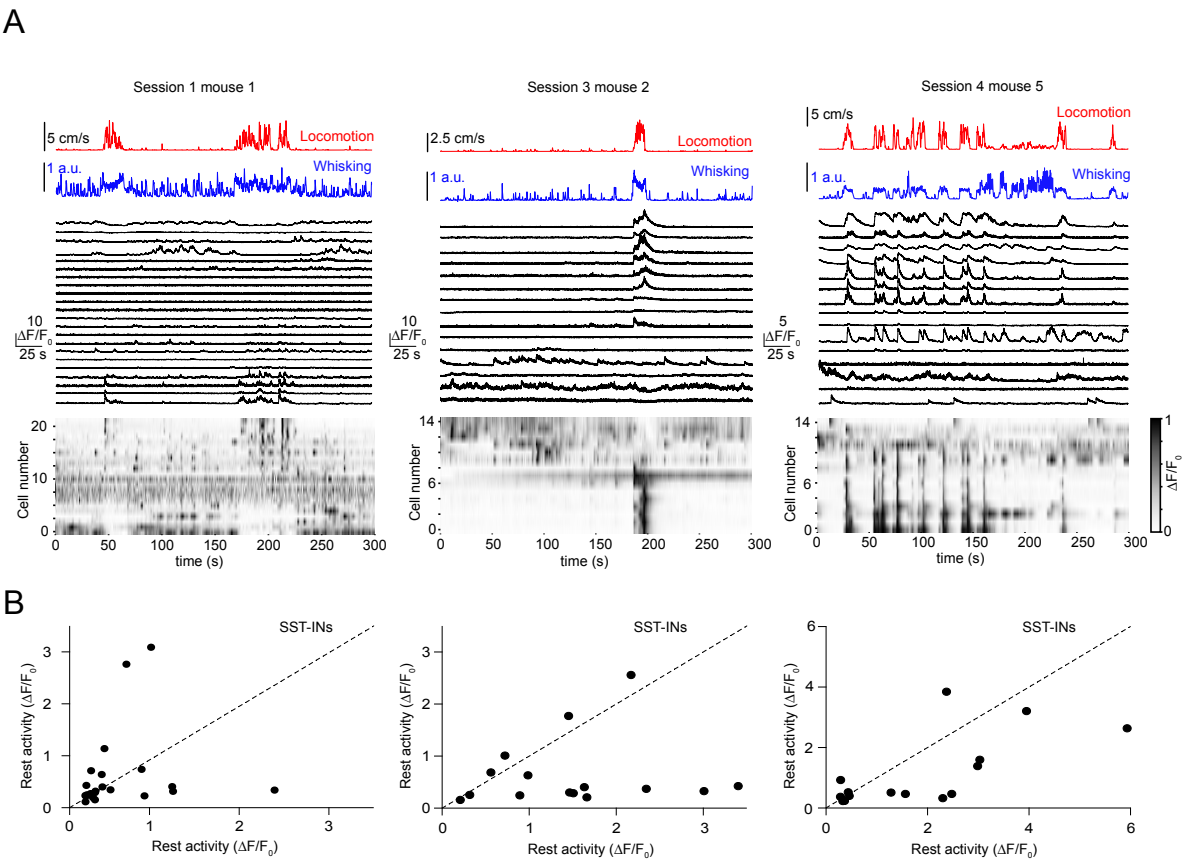

Supplementary figure 1: Variability of SST-INs response within individual fields of view in S1 to behavioral transitions from rest to run. A) Representative GCaMP6s fluorescence traces (black) shown as $\Delta F/F_0$ (up) as well as normalized $\Delta F/F_0$ (bottom) for SST-INs for individual fields recorded in awake mice spontaneously transitioning between rest and run periods. Each row represents a neuron sorted by weight on the first principal component (PC) of their activity. Locomotion (red) and whisking (blues) traces are shown on top. **B)** Scatter plots of the mean amplitude of fluorescence changes (DF/F_0) of each neuron illustrated in A for locomotion periods versus stationary periods.

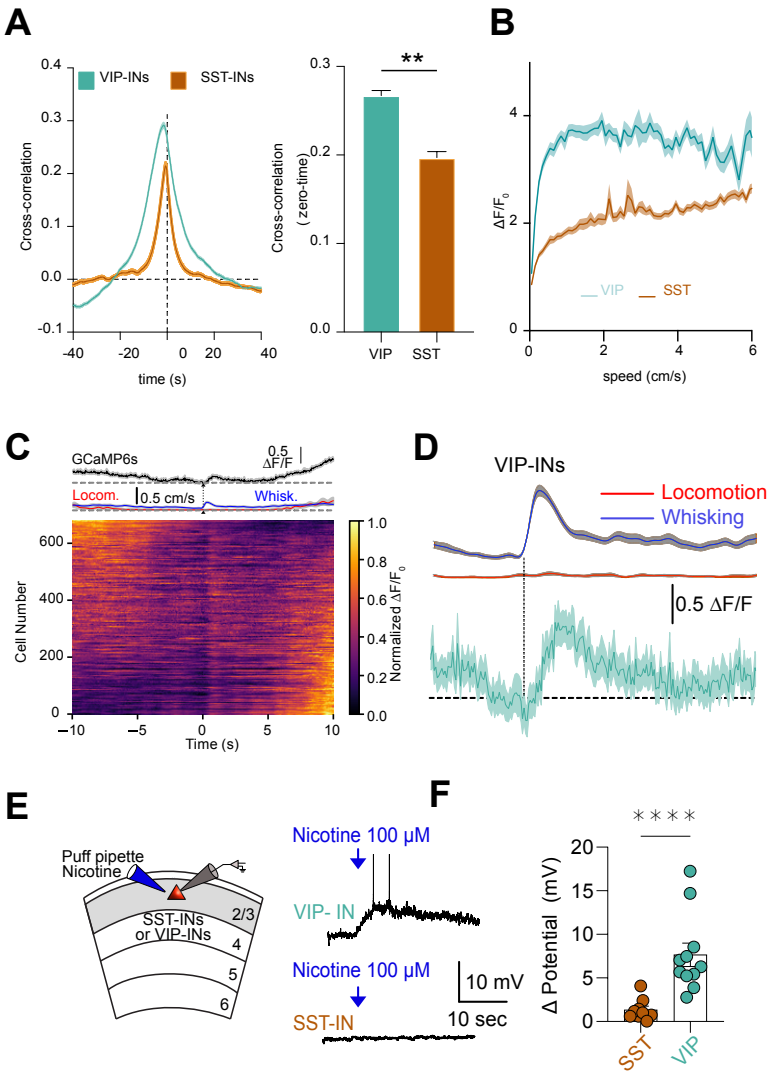

Supplementary figure 2: Response of SST- and VIP-INs in S1 to behavioral transitions from rest to run. A) Cross-correlation curves between running speed and calcium activity for VIP and SST-INs. Values at zero time are displayed on the right. **B)** Variation in ΔF/F values for SST- and VIP-INs with average running speed. **B)** Event-triggered average traces of VIP-INs GCaMP6s fluorescence signal in S1 aligned to whisking onset. Only whisking bouts not associated with locomotion were used (whisking only). Normalized ΔF/F is displayed for all analyzed cells (bottom). Traces represent mean ± SEM values across all recorded cells. **(C)** Enlarged view of average traces shown in A. **B)** Schematic illustration of whole-cell current clamp recording in L2/3 of primary somatosensory (S1) cortex while puff applying nicotine 100 ⌈M in SST or VIP-INs (left). Example traces of puff-evoked responses in SST- and VIP-INs (right). **C)** Summary plot of variations in membrane potential induced by nicotine applications in both SST- and VIP-INs (SST [n = 11] vs VIP [n = 9], $p < 0.0001$, Mann-Whitney test).

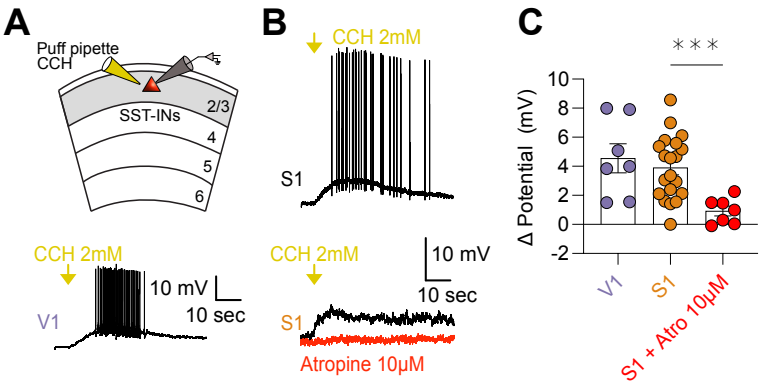

Supplementary figure 3: SST-INs are equipped with cholinergic receptors in both V1 and S1.

A) Schematic illustration of whole-cell current clamp recording in L2/3 of primary somatosensory (S1) cortex while puff applying carbachol (2mM) in SST (up). Example traces of puff-evoked responses in SST-INs (down). **B)** Example traces of current clamp recordings illustrating the variation in membrane potential in SST-INs to puff application of carbachol in both V1 (P>56: top right) and S1 (P<56 middle right; P>56 bottom right). **C)** Summary plot of the variation of membrane potential induced by carbachol (CCH) in SST-INs in V1 and S1 (V1, SST [n = 7]; S1, SST with CCH puff alone [n = 20] versus SST with CCH puff in the presence of atropine 10⌠M [n = 7], p = 0.007, Mann-Whitney test)**.** Error bars are SEM.

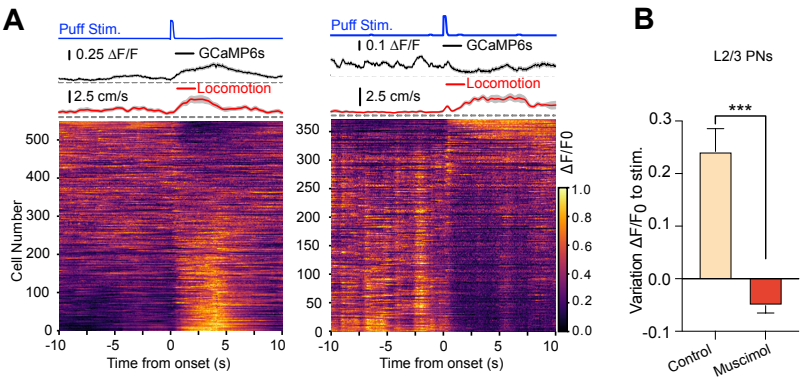

Supplementary figure 4: Somatosensory thalamus inactivation with muscimol injection decreases whisker-evoked pyramidal cell activity in S1. A) Event-triggered average traces of L2/3 PNs GCaMP6s signals in S1 aligned to whisker puff along with running speed (red). Normalized ΔF/F is displayed for all analyzed cells (bottom). Results are displayed for control conditions (left) and for mice previously injected with muscimol in the thalamus (*right*). Traces represent mean ± SEM values across all recorded cells. **B)** Summary plot of variation in ΔF/F between rest and after whisker stimulation for the event-triggered average traces shown in B. Average values were obtained 2 s before and 2 s after whisker stimulation onset (see Methods).

1024 **Experimental Procedures:**
1025
1026 **Mice:**
1027
1028 Animals were housed in the Paris Brain Institute accredited by the French Ministry of
1029 Agriculture. All experiments were performed in compliance with French and European regulations
1030 on care and protection of laboratory animals (EU Directive 2010/63, French Law 2013-118,
1031 February 6th, 2013), and were approved by local ethics committees and by the French Ministry
1032 of Research and Innovation (authorization numbers #11199). All animal work was performed at
1033 the ICM PHENO-ICMice facility. Both male and female mice aged 4 weeks or older were used
1034 with the following genotypes: SST-IRES-Cre (SSTtm2.1(cre)Zjh/J; JAX 013044); SST-IRES-Cre
1035 X Ai9 (Gt(ROSA)26Sortm9(CAG-tdTomato); JAX 007909); VIP-IRES-Cre
1036 (Viptm1(cre)Zjh/AreckJ; JAX 031628) X Ai9 (Gt(ROSA)26Sortm9(CAG-tdTomato); JAX 007909);
1037 VIP-cre::SST-FLP (*Sst*$^{tm3.1(flpo)Zjh}$/J; JAX 028579). Animals were maintained on a 12-hour light/dark
1038 cycles with food and water provided ad libitum. Animals were housed in groups of 2-6 animals
1039 per cage, as often as possible, to favor social interactions, a condition that prevents the
1040 emergence of depressive and anxious-like behavior (Berry et al., 2012; Ieraci et al., 2016; Kappel
1041 et al., 2017).
1042
1043 **Slice preparation**
1044 Acute parasagittal slices (320 μm) were prepared from adult mice, starting from postnatal
1045 days 25–70. Mice were deeply anesthetized with a mix of ketamine/xylazine (mix of i.p. ketamine
1046 16 mg/kg and xylazine 13 mg/kg) and perfused transcardially with ice-cold cutting solution
1047 containing the following (in mM): 220 Sucrose, 11 Glucose, 2.5 KCl,1.25 NaH2PO4, 25 NaHCO3,
1048 7 MgSO4, 0.5 CaCl2. After the perfusion the brain was quickly removed and slices prepared using
1049 a vibratome (Leica VT1200S). Slices containing S1 barrel field or V1 were transferred to ACSF
1050 solution at 34 °C containing (in mM): 125 NaCl, 2.5 KCl, 2 CaCl2, 1 MgCl2, 1.25 NaH2PO4, 25

1051 NaHCO3, 15 Glucose for 15–20 min. After the period of recovery, slices were kept at room
1052 temperature for a period of 5-6 h.
1053
1054 **Electrophysiology:**
1055 Whole-cell patch-clamp recordings were performed close to physiological temperature
1056 (32–34 °C) using a Multiclamp 700B amplifier (Molecular Devices) and fire-polished thick-walled
1057 glass patch electrodes (1.85 mm OD, 0.84 mm ID, World Precision Instruments); 3.5–5 MOhm
1058 tip resistance. For voltage-clamp recordings, cells were whole-cell patched using following
1059 intracellular solution (in mM): 90 Cs-MeSO3, 10 EGTA, 40 HEPES, 4 MgCl2, 5 QX-314, 2.5
1060 CaCl2,10 Na2Phosphocreatine, 0.3 MgGTP, 4 Na2ATP (300 mOsm pH adjusted to 7.3 using
1061 CsOH). Extracellular synaptic stimulation was achieved by applying voltage pulses (20 us, 5–50
1062 V; Digitimer Ltd, UK) via a second patch pipette filled with ACSF and placed 20–40 mm from
1063 soma. For current clamp experiments patch pipettes were filled with the following intracellular
1064 solution (in mM): 135 K-gluconate, 5 KCl, 10 HEPES, 0.01 EGTA, 10 Na2phosphocreatine, 4
1065 MgATP, 0.3 NaGTP (295 mOsm, pH adjusted to 7.3 using KOH). The membrane potential (Vm)
1066 was held at -60 mV, if necessary, using small current injection (typically in a range between -50
1067 pA and 200 pA). Recordings were not corrected for liquid junction potential. Series resistance was
1068 compensated online by balancing the bridge and compensating pipette capacitance. APs were
1069 initiated by brief current injection ranging from 1000–2000 pA and 1–5 ms duration. For all
1070 experiments data were discarded if series resistance, measured with a 10 mV pulse in voltage
1071 clamp configuration, was >20 MOhm or changed by more than 20% across the course of an
1072 experiment. For current clamp experiment cells were excluded if input resistance varied by more
1073 than 25% of the initial value. Recordings of puff evoked cholinergic responses in SST- and VIP-
1074 INs were performed at the resting membrane potential in the presence of 10 μM CNQX and 10
1075 μM bicuculine.

1076 All recordings were low-pass filtered at 10 kHz and digitized at 100 kHz using an analog-
1077 to-digital converter (model NI USB 6259, National Instruments, Austin, TX, USA) and acquired
1078 with Nclamp software (Rothman and Silver, 2018) running in Igor PRO (Wavemetrics, Lake
1079 Oswego, OR, USA). The intracellular solution used for the experiments in which a presynaptic
1080 cell was depolarized by a train of action potentials to induce neurotransmitter release on a post-
1081 synaptic cell/element was (in mM): 130 K-MeSO3, 4 MgCl2,10 HEPES, 0.01 EGTA, 4 Na2ATP,
1082 0.3 NaGTP (300 mOsm, pH 7.3 adjusted with NaOH). Paired recordings connections were probed
1083 using a train of 5/9 action potentials at frequency of 20 Hz.
1084

1085 **In vivo two-photon calcium imaging**

1086 **Surgery**

1087 Mice were initially anesthetized with Isoflurane. Induction of anaesthesia was performed
1088 at 4% isoflurane, Iso-Vet, and an air flow of 250ml/min. Mice were then placed in a stereotactic
1089 device (Kopf) kept at 37 °C using a regulated heating blanket and a thermal probe and maintained
1090 under anaesthesia using 1-2% Isoflurane and an air flow of 250 ml/min until the end of the
1091 surgery. For calcium imaging in VIP- and SST-INs, cranial window implantation and AAV viral
1092 stereotaxic injection was performed in the same surgical procedure. In order to prevent brain
1093 swelling and post-operative pain, anti-inflammatory (Dexamethasone, 2 µg/g Dexadreson, MSD)
1094 and analgesic drugs (Buprenorphine, 0.1 mg/kg Buprecare) were injected subcutaneously. After
1095 shaving the scalp, the skin was cleaned by wiping multiple times with an antiseptic solution and
1096 70% alcohol. After injecting a local anaesthetic under the scalp (lidocaine, 10mg/kg - Xylovet or
1097 Laocaine) a section of the skin (a circular section with 1.5 cm diameter) was removed using
1098 surgical scissors. The periosteum was then carefully removed and the skull was scrapped using
1099 a dental drill, in order to remove all residues. The surface of the skull was subsequently thoroughly
1100 cleaned and dried using cottons swabs and a physiological saline solution. Using the stereotactic

1101 device, the center of the cranial window was marked and a circular piece of bone was removed
1102 using a 3 mm biopsy punch (LCH-PUK-30 Kai Medical). This step of the surgical procedure was
1103 considered critical since damage to the dura would result in rapidly opacifying cranial windows.
1104 Once the brain was exposed, the AAV viral vectors carrying the genetically encoded calcium
1105 indicators (GCaMP6 f and s) were stereotactically injected. For calcium imaging of VIP-INs, SST-
1106 INs and pyramidal neurons, AAV9 Syn-Flex-GCaMP6f-WPRE-SV40 ($2.1x10^{13}$ AddGene-
1107 100833), AAV9 Syn-Flex-GCaMP6s-WPRE-SV40 ($2.5x10^{13}$ AddGene-100845) or AAV9 ENN-
1108 AAV-CaMKII.GCaMP6f-WPRE-SV40 ($2.5x10^{13}$ AddGene-100834) was used respectively. Using
1109 a Nanojet III (Drummond Scientific), 200nl of virus were injected in the barrel cortex (from Bregma,
1110 1.1 RC; 3.3 ML) or visual cortex (from bregma: 3.0 RC; 2.4 ML) at a rate of 1nl/s followed by 5
1111 minutes of wait to prevent backflow. A round of 3mm glass coverslip (CS-3R Warner Instruments)
1112 was then placed over the craniotomy and glued in place using dental cement (Superbond). A
1113 stainless-steel head post (Luigs & Neumann) was then attached to the skull also using dental
1114 cement. For 3 days following the cranial windows surgery, mice were injected once a day with a
1115 mix of anti-inflammatory (Dexamethasone, 2μg g^{-1} Dexadreson, MSD) and analgesic drugs
1116 (Buprenorphine, 0.1 mg/kg Buprecare). Two weeks after surgery, mice were first habituated to
1117 the experimenter by handling. The following days, mice were head-fixed in the acquisition setup
1118 for increasing periods of time (5 – 45 minutes).

1119 **Thalamus inactivation**

1120 In order to inactivate the somatosensory-associated thalamus, following the acquisition of
1121 several control imaging sessions, mice were placed in a stereotactic device, and put under light
1122 isoflurane anesthesia. A hole was drilled over the ipsilateral thalamus and using a cannula, a
1123 bolus of fluorescent Muscimol (0.5 mM, Muscimol, BODIPY™ TMR-X Conjugate Muscimol,
1124 BODIPY™ TMR-X Conjugate, ThermoFischer Scientific) was slowly injected into the thalamus
1125 (Coordinates: -1.82 RC, 1.5 ML, 3.5 depth). After injection, the craniotomy was covered with

1126 silicone (Kwik-Cast, WPI) and the mouse was allowed to recover for an additional 30 minutes.
1127 After recovery, two-photon imaging was performed for a maximum of one hour post muscimol
1128 injection. The effective inactivation of the thalamus was confirmed functionally by recording the
1129 response of pyramidal cells as well as local cortical interneurons to whisker stimulation as well as
1130 by performing histology just after the imaging sessions.

1131 **Two-Photon Imaging**

1132 In vivo two-photon calcium imaging was performed with an Ultima IV two-photon laser-
1133 scanning microscope system (Bruker), using a 20×, 1.0 N.A. water immersion objective (Olympus)
1134 with the femtosecond laser (MaiTai DeepSee, Spectra Physics) tuned to 920 nm for imaging of
1135 cells expressing GCaMP6s/f and to 1020 nm for imaging of cells expressing mCherry.
1136 Fluorescence light was separated from the excitation path through a long pass dichroic (660dcxr;
1137 Chroma, USA), split into green and red channels with a second long pass dichroic (575dcxr;
1138 Chroma, USA), and cleaned up with band pass filters (hq525/70 and hq607/45; Chroma, USA).
1139 Fluorescence was detected using both proximal epifluorescence photomultiplier tubes (gallium
1140 arsenide phosphide, H7422PA-40 SEL, Hamamatsu). Time-series movies of neuronal
1141 populations expressing GCaMP6f were acquired at the frame rate of 30Hz (512 × 512 pixels field
1142 of view; 1.13 μm/pixel). The duration of each focal plane movie was 300s (9000 frames) to track
1143 spontaneous neuronal activity. During the recording periods animals were free to run on a circular
1144 treadmill covered with a soft foam. This foam softened the movement of the animals and provided
1145 better traction (this was important since mice adapted more rapidly to the experimental setup and
1146 movements were more fluid during the recordings). Locomotion was monitored using a rotary
1147 encoder (H5-1000-NE-S, US Digital) and digitized with a NIDAQ analog-to-digital converter
1148 (model NI USB 6363, National Instruments, Austin, TX, USA) at 2000 Hz. Whisker movement
1149 was recorded using a FLIR camera (BFS-U3-17S7M-C) at a frame rate of 30Hz and using the
1150 Spinnaker SDK software (FLIR Systems Inc, Orlando, USA) equipped with a cleanup filter

1151 (FB850-40, Thor labs) to block laser shining from during two-photon imaging. The camera was
1152 focused on the whisker pad of the mouse using a 10X (13 - 130mm FL) C-Mount, Close Focus
1153 Zoom lens and each frame acquisition was controlled via Neuromatic running in IGORPRO
1154 (Wavemetrics) environment using a national instruments digital-to-analog board (NI-6393). The
1155 mouse snout was illuminated via an 850 nm LED (M850L3, Thor labs).

1156 **Whisker Stimulation**

1157 For whisker stimulation experiments, a NPI PDES-02DX (NPI Electronic GmbH) puffer
1158 was used. Tubing was connected to the puffer and a short puff (1 sec) of air was aimed at the
1159 mouse whiskers. The tip of the puffer was kept out of reach of exploratory whisking range. The
1160 whisker puff was randomly triggered during imaging sessions and the time of puff was recorded
1161 via the digitization of voltage trigger using a analog-to-digital converter (model NI USB 6259,
1162 National Instruments, Austin, TX, USA)

1163 **CNO Experiments:**

1164 For experiments involving DREADDs, mice were injected with clozapine-N-oxide (CNO).
1165 A water-soluble salt preparation of CNO, CNO dihydrochloride (Tocris, Bio-Techne LTD,
1166 Abingdon, UK, catalog no.: 6329), which was dissolved in sterile saline. Several concentrations
1167 of CNO were tested (1, 5 and 10mg/kg) and no significant changes were found so data was all
1168 data was pulled together.

1169 **Visual stimulation**

1170 To study the effect of light on the recruitment of VIP- and SST-INs in the cortex, an
1171 isoluminant grey screen (Lilliput 669GL 7”) was placed at 45° from the center line of the mouse
1172 and at approximately 20cm from the left eye (contralateral to the craniotomy) of the mouse. Visual
1173 stimulation trials were interleaved with control trials. In order to reduce light contamination, a
1174 custom funnel was used to shield the objective from light coming from the screen.

1175 **Calcium Imaging Analysis**

1176 **Motion correction, Image segmentation and calcium signal extraction**

1177 Motion correction, image segmentation and calcium signal extraction were performed
1178 using the python 3.6 package Suite2P (Pachitariu et al., 2016). This package analyses data in
1179 four stages: image registration, region of interest (ROI) detection, quality control, and activity and
1180 neuropil extraction. The first stage, image registration, is responsible for motion correction and
1181 works by performing a mean image of a few frames and then shifting (in the x and y axis) each
1182 frame so that it optimally fits the mean image. The second stage, ROI detection, detects the cells
1183 in the frame. This is done by detecting the pixels with the highest variability across time and then
1184 expanding the region to the surrounding pixels until this variability drops below a defined
1185 threshold. Although this method works quite well, the disadvantage of this method is that since
1186 only active cells are detected, it is difficult to determine the number of silent cells in field of view,
1187 which could be important for functional tasks. In a third stage, quality control, the program
1188 separates structures that correspond to cells from the remaining structures by assigning them a
1189 score. The results of this stage were always manually curated. In the last stage of the analysis,
1190 activity and neuropil extraction, is performed by averaging the pixel intensity in the ROI for each
1191 time point. To determine the neuropil, a donut-like surrounding the ROI is generated and the
1192 activity within this area is also averaged for each time point. Neuropil plays a critical role in calcium
1193 imaging since it represents the activity of nearby structures surrounding the cell of interest that
1194 might be excited by the 2P excitation PSF. Since these structures might have a different
1195 behavioral profile than the cell of interest their activity might contaminate the signals detected in
1196 the cell soma (Dipoppa et al., 2018).

1197 **Analysis of fluorescence signals**

1198 Raw fluorescence traces were corrected for neuropil contamination by subtracting
1199 Suite2p-neuropil traces using a fixed scaling coefficient of 0.7 (Dipoppa et al., 2018). To be able
1200 to compare activity across cells and mouse lines, fluorescence signals were normalized. To do
1201 this we used the $\Delta F/F_0$ method, calculated using the following formula: $(F-F_0)/F_0$, where F is the
1202 fluorescence and F_0 is the baseline fluorescence. When studying the activity of interneurons (VIP-
1203 and SST-INs), the baseline fluorescence was calculated using the lower 5th percentile. Results
1204 were systematically evaluated using a different baseline method to estimate F0 (MinMax baseline
1205 method with a sliding window of 60s) and observations reported in the present manuscript were
1206 insensitive to the baseline method used. For the analysis of pyramidal cell activity, a sliding
1207 average window (60 s) defined as MinMax method was used.

1208 **Locomotion Analysis**

1209 Changes in positioning of the circular treadmill (sampled at 2 kHz) were interpolated onto
1210 a down-sampled rate of 30Hz in order to match the sampling rate of the two-photon imaging.
1211 Locomotion periods, were defined as the periods where speed was higher than 0.1 cm/s. All
1212 points 0.5 seconds before and 1.5 seconds after a locomotion period were considered stationary
1213 periods. Events spaced by less than 0.5s were joined. Sessions in which the percentage of either
1214 locomotion or stationary periods were lower than 5%, were excluded. The locomotion modulation
1215 index (LMI) was defined as the difference between the mean $\Delta F/F_0$ during locomotion (F_{run}) and
1216 stationary (F_{rest}) periods, normalized by the sum of both values: $LMI = (F_{run} – F_{rest})/(F_{run} + F_{rest})$
1217 (Pakan et al., 2016). To calculate statistically significant Pearson Correlations between
1218 fluorescence and running speed, comparisons were made with 1000 shuffled (circular shuffling)
1219 locomotion traces. Pearson correlation coefficient was considered statistically significant if value
1220 of original data was above a 95% confidence interval generated from the 1000 shuffled traces.

1221 **Whisking Analysis**

1222 Whisker pad movement was tracked using the python framework Facemap (Syeda et al.,
1223 2022) (https://github.com/MouseLand/facemap). Whisker-pad movement was measured by
1224 selecting an ROI over the whisker pad and calculating the motion energy index (MEI) across the
1225 video. MEI was defined as the sum of the absolute change in pixel intensity within the ROI
1226 between adjacent video frames. Using custom python code, whisking pad motion energy was
1227 filtered with a gaussian filter (sigma of 3), normalized with a Min Max method and resampled to
1228 30Hz. Whisking periods were defined as periods where normalized MEI exceeded 10 %. Whisking
1229 only periods were defined as periods in which there was whisking but not locomotion. Whisking
1230 modulation index (WMI) and whisking only modulation index (WOMI) were calculated in a similar
1231 way to LMI but using the variations in GCaMP6s fluorescence during resting or whisking periods.

1232 Event-triggered averages were computed by automatically identifying frames with event
1233 onsets, namely those related to whisking and/or locomotion. Due to the slow time course of
1234 GCaMP6s and to minimize cross-talk between events, we specifically chose locomotion events
1235 that were not preceded by another locomotion period within a 5-second interval. For whisking only
1236 analysis, whisking episodes not associated with locomotion were included in the average (5se
1237 before and 5 sec after). In Figure 3I, locomotion events were further categorized in agreement
1238 with locomotion duration. Once multiple locomotion and/or whisking events were detected, the
1239 results were combined and averaged to calculate an average value for each cell. Subsequently,
1240 these individual average cell values were averaged together and presented with their respective
1241 average and SEM.

1242

1243 **Statistics**

1244 All statistical analysis were performed in Prism (GraphPad Software, Inc.). The error bars
1245 in all graphs indicate standard error of the mean (S.E.M.) and statistics were performed with two-

tailed tests. For statistical tests comparing the average $\Delta F/F_0$ of neurons between two behavioral states (stationary versus locomotion periods) in the same subject, we used Wilcoxon signed-rank tests. For statistical tests comparing the distribution of LMI, Pearson Correlation or behavior properties between brain regions or interneuron populations, Mann-Whitney U tests were used. When comparing two conditions across behavioral states, Kruskal-Wallis test was used.